Pure Appl. Geophys. 183 (2026), 3291–3320

https://doi.org/10.1007/s00024-026-04011-1

Pure and Applied Geophysics

Impact of November 2023 Storms along the Southern Black Sea Coastline

Hasan Gokhan Guler,[1] Gozde Guney Dogan,[1,2] Isikhan Guler,[1] Cagil Kirezci,[3,4] Seyda Pirincci,[5] and Ahmet Cevdet Yalciner[1]

Abstract—This study presents a comprehensive assessment of two successive storm events that impacted the Black Sea coasts in November 2023. Using a combination of meteorological and oceanographic datasets, satellite altimetry, and an extensive post-disaster field survey conducted at most of the affected regions along the Southern Black Sea coastline, the characteristics of storms and their impacts on coastal structures and communities are documented in detail. The storms, spaced just one week apart, generated significant wave heights exceeding 7–8 m offshore, wind speeds above 20–25 m/s, and widespread coastal inundation. Despite the limitations in the spatial resolution of global datasets, particularly in capturing localized wind and wave conditions, datasets provided valuable insights together with observational data. Field observations revealed recurring structural damages across the region, particularly the breakwater crown walls, due to high wave impact. At several harbors, displaced armor units contributed to damage. Inundation extends up to 270 m, highlighting the extreme wave run-up and overtopping during the storms. A digital repository containing photos and videos was also developed and openly shared via the Zenodo platform to support further research and documentation. This study contributes a unique and open-access dataset, empirical insights on structural damage mechanisms, and a baseline for improving future coastal hazard assessments in semi-enclosed seas such as the Black Sea.

Keywords: Black Sea, storm, damage, inundation, breakwater, november 2023.

[1] Department of Civil Engineering, Coastal and Ocean Engineering Division, Middle East Technical University, 06800 Ankara, Türkiye. E-mail: goguler@metu.edu.tr; gguneydogan@gmail.com; isikhan@metu.edu.tr; yalciner@metu.edu.tr

[2] Department of Hydraulic Engineering, Delft University of Technology, 2628, CN, Delft, The Netherlands.

[3] CSIRO Environment, 3195 Aspendale, VIC, Australia. E-mail: cagil.kirezci@unimelb.edu.au

[4] Infrastructure Engineering, University of Melbourne, Parkville, Australia.

[5] Ministry of Transport and Infrastructure, XI. Regional Directorate, 61100 Trabzon, Türkiye. E-mail: seydapirincci@uab.gov.tr

1. Introduction

As part of the broader extreme weather events that impacted Europe in November 2023, two notable storms occurred in the Black Sea on November 18–19 and November 26–27, 2023, which caused human casualties and economic loss along the Black Sea coast of Turkiye. Wind speeds reached up to 25–30 m/s, accompanied by significant storm surges as well as combined swell and wind waves exceeding 7–8 m based on European Centre for Medium-Range Weather Forecasts (ECMWF) ERA5 reanalysis dataset (Hersbach et al., 2020). Significant coastal inundation was observed at several locations, resulting in damage at the (mostly recreational) facilities located near the shoreline. Several mound breakwaters protecting both commercial harbors and fishery harbors suffered from severe damage. Also, several commercial ships sank or grounded due to high nearshore waves and strong currents.

In the Black Sea region, destructive storms are frequently observed (Bernardino et al., 2021), which cause coastal flooding, damage to ports, and ship damage. In recent years, numerous studies focused on the storms and their effects in the Black Sea region. For instance, Fashchuk (2007) analysed an oil spill event due to breakage of the tanker Volgoneft-139 in the Kerch Strait (located at the Northern Black Sea) during a significant storm on November 8–10, 2007. Aydin (2014) carried out a comparative study using several numerical models, to assess a storm severely affected Southeastern Black Sea coast on September 23–24, 2014, where up to 5 m run-up heights were estimated. More recently, Amarouche et al. (2024) examined the characteristics of storm events in the Black Sea, concluding that Turkish ports along the southern Black Sea coastline, as well as the ports of

Novorossiysk and Sevastopol in the north, have experienced the most frequent storm exposure over the past 42 years. As an example, Guler et al. (2024) recently presented an investigation of the major damage at a port located at the Southwestern Black Sea (including failure of breakwaters), due to a severe storm on January 18–19, 2018. Additionally, Vilibić et al. (2010) classified a shelf tsunami, which caused slight damage at several regions in Bulgaria (Ranguelov et al., 2007), as a meteotsunami event occurred on May 7, 2007, based on the evidence of the travelling atmospheric disturbance in the investigated dataset. One of the distinctive aspects of the November 2023 storms is that two significant storms struck just one week apart. While these storms were separated by a brief calm period (and thus can be treated as distinct events), their back-to-back occurrence strained regional emergency response and drew attention to the possibility of repeating extremes in relatively short durations.

In the present study, we report and evaluate the damage and coastal inundation due to these two successive significant storms occurred in November 2023 in the Black Sea, concentrating on the coastline of Turkiye. The investigations and discussions are based on assessment of available meteorological and oceanographic data, in addition to the four field surveys, covering most of the affected regions. Fig. 1a presents an overview of the Black Sea region, together with the locations of several meteorological and oceanographic data points. The first storm (November 18–19, 2023) mainly affected a region between 27.5°E and 32.5°E longitudes along the Southern Black Sea coastline (Fig. 1b). On the other hand, the second storm (November 26–27, 2023) significantly affected a region between 33.0°E and 41.8°E longitudes along the Southern Black Sea coastline (Fig. 1c). These affected regions were identified based on observed inundation and damage events, which were confirmed during the field investigations through personal communication with local governmental authorities and eyewitnesses.

A unique contribution of this work lies in the dataset compiled during the field studies, which includes coastal inundation measurements, damage mapping, drone imagery, and eyewitness documentation. Analysis of structural damage revealed consistent failure mechanisms at multiple harbors. These findings not only expose a common vulnerability in existing coastal defenses but also underscore the critical role of site-specific post-event surveys in validating storm hazard assessments and informing future coastal engineering practices.

This study is structured as follows: After this brief introduction, the available meteorological and oceanographic data are evaluated in Section 2. In Section 3, the field observations are reported. Finally, the discussions and conclusions are given in Section 4 based on the information gathered from the available datasets and field observations.

2. *Evaluation of Meteorological and Oceanographic Data*

2.1. *Wind Data*

In the present study, the wind data investigations are based on in-situ wind speeds from coastal meteorological stations (CMS) and the European Centre for Medium-Range Weather Forecasts (ECMWF) ERA5 reanalysis dataset (Hersbach et al., 2020). In-situ wind speed data is presented for three CMSs first; subsequently, wind speeds and directions are discussed based on the ECMWF-ERA5 reanalysis dataset to describe the overall situation in the Black Sea during both storms.

The in-situ CMS data are provided at 10 m above the sea level at locations shown in Fig. 1. For the first storm, wind data from Akçakoca Lighthouse (CMS-1, located at 41.0922°N, 31.1197°E) and Bartın South Breakwater (CMS-2, located at 41.6864°N, 32.2261°E) are taken into account, whereas wind data from Trabzon Breakwater (CMS-3, located at 41.0075°N, 39.7500°E) is used for the second storm. Although there are many CMSs along the Southern Black Sea coastline, these stations are specifically selected due to two reasons: (i) All three stations are placed on the breakwaters; therefore, the measurements are not significantly affected by local effects (buildings, vegetation, etc.). (ii) The storms are fully recorded only by these stations among the other CMSs along the Southern Black Sea coastline, which are also placed on the breakwaters. The wind speed

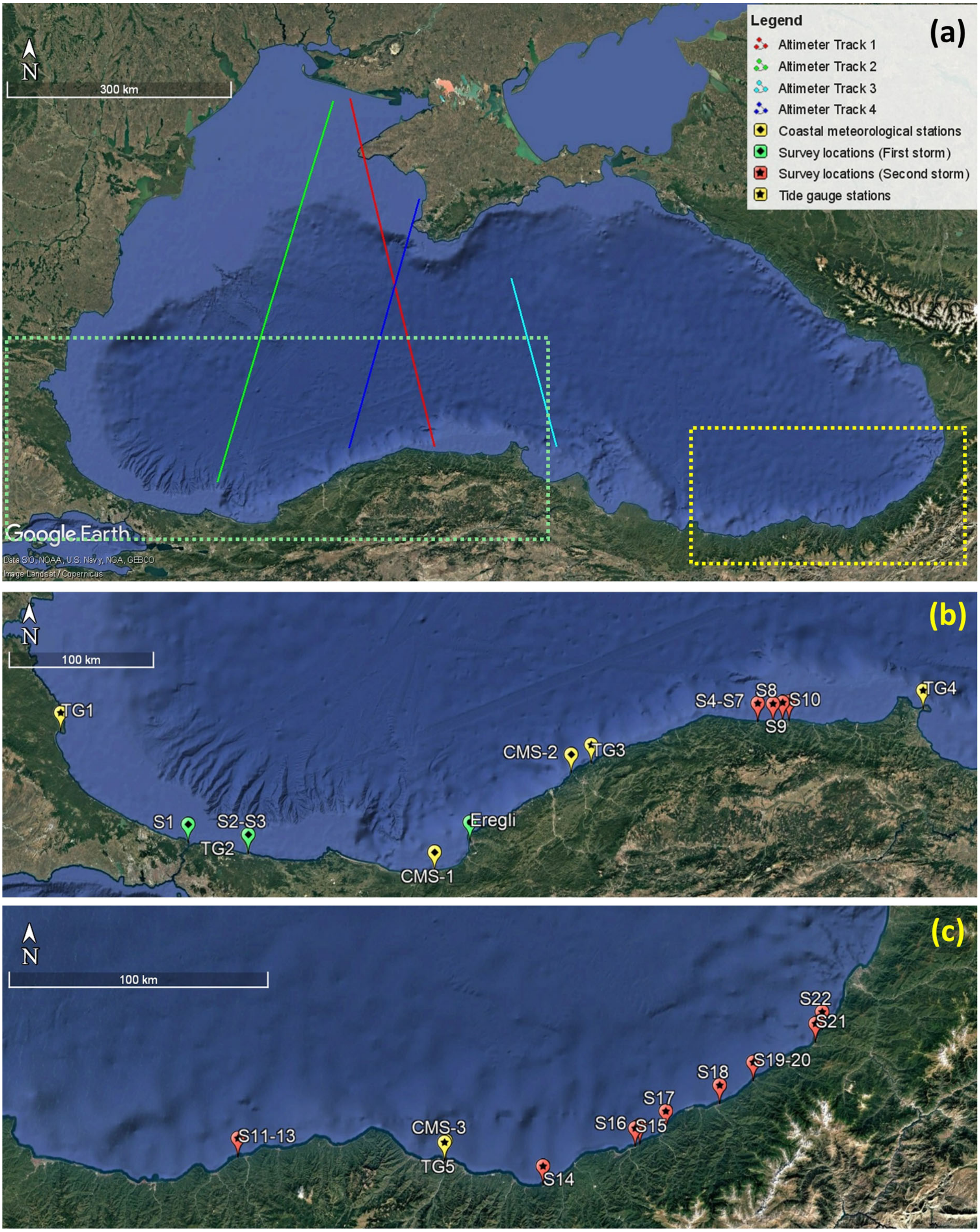
Legend
(a)
Altimeter Track 1
Altimeter Track 2
Altimeter Track 3
Altimeter Track 4
Coastal meteorological stations
Survey locations (First storm)
Survey locations (Second storm)
Tide gauge stations
N
300 km
Google Earth
(b)
100 km
TG1
S1
S2-S3
TG2
CMS-1
Eregli
CMS-2
TG3
S4-S7
S8
S9
S10
TG4
(c)
100 km
S11-13
CMS-3
TG5
S14
S16
S15
S17
S18
S19-20
S21
S22

◀Figure 1
Satellite (Google Earth) imagery of the study area in the Black Sea, showing data collection locations: **a** Overview of the entire Black Sea Region, indicating altimeter tracks (Track 1-Sentinel 3A: red solid line, Track 2-Sentinel 3B: green solid line, Track 3-Sentinel 3A: light blue solid line, Track 4-Sentinel 3B: dark blue solid line). The green and yellow dashed rectangles correspond to the regions shown in panels b and c, respectively. **b** Detailed view of field survey locations (denoted by S), tide gauge locations (TG), and coastal meteorological station locations (CMS) (corresponding to the green rectangle in panel (a)). **c** Detailed view of field survey locations, TG and CMS points in the Eastern Black Sea region (corresponding to the yellow rectangle in panel (a)). (The Google Earth kmz file of this figure is provided in the data repository. See the Data Availability Statement)

time series from these stations are presented in Fig. 2, noting that the CMS data has a temporal interval of 60 sec, which was averaged over one hour for presentation purposes. Regarding the first storm, the in-situ measurements show two peaks at the Akçakoca Lighthouse and Bartın South Breakwater CMSs. At Akçakoca Lighthouse CMS, the first peak was around 16 m/s for two hours, whereas the second peak was around 17–18 m/s and lasted for approximately five hours. Moreover, the first peak at the Bartın South Breakwater exceeded 16 m/s for two hours, and the second peak at this CMS was around 17 m/s for a single hour. On the other hand, a single peak with a magnitude of approximately 15 m/s was observed at the Trabzon Breakwater CMS for about three hours during the second storm.

The overall variation of the wind speeds and directions for both storms are presented based on hourly ECMWF-ERA5 reanalysis dataset, having a spatial resolution of 0.25°. This reanalysis dataset is specifically selected, as it is frequently used for research and engineering purposes in the Black Sea (see e.g. Guler et al. (2024)). As there are no publicly available offshore wind measurements during the event in the Black Sea region to the authors' knowledge, ECMWF's ERA5 wind speed data is compared against altimeter data. During both storms, Sentinel 3A and 3B altimeters passed through the Black Sea region. The altimeter tracks during the storms are shown in Fig. 1a, while detailed information on those tracks is presented in Table 1. The comparisons carried out by linearly interpolating the data from ERA5 both in spatial and time domains based on the altimeter track coordinates and passage time. In the comparisons, the altimeter data points at least 20 km away from the coastline were considered,

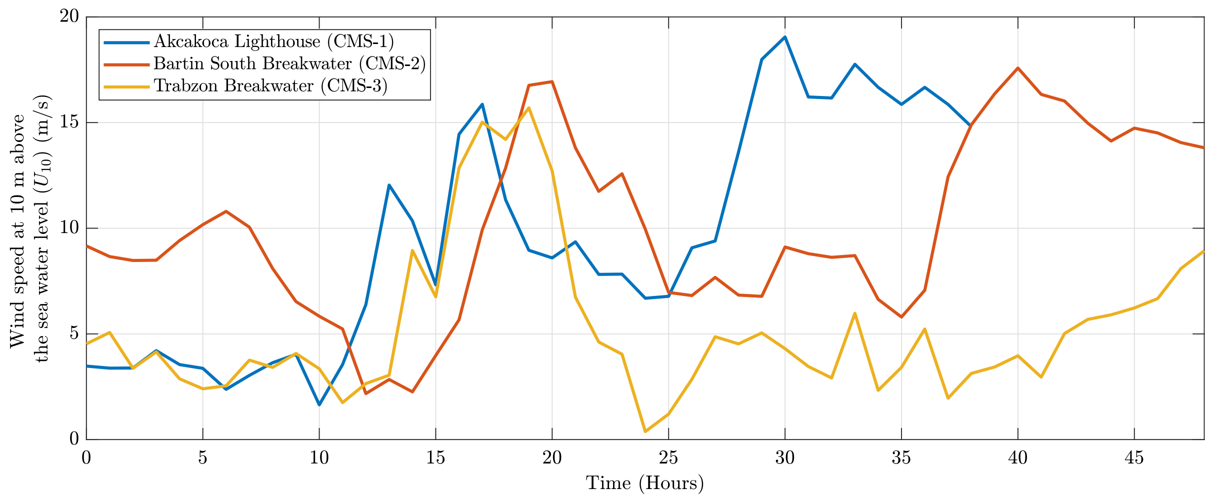

Figure 2
In-situ wind speed data from coastal meteorological stations (CMS): Akçakoca Lighthouse (CMS-1, blue solid line) and Bartın South Breakwater (CMS-2, red solid line) for the first storm (November 18–19, 2023), Trabzon Breakwater (CMS-3, yellow solid line) for the second storm (November 26–27, 2023). (0^{th} hour corresponds to November 18, 2023, 00:00 UTC and November 26, 2023, 00:00 UTC for the first and second storms, respectively. It is noted that the length of the data for Akcakoca Lighthouse CMS is just 39 h whereas it is 48 h for other CMSs)

Table 1

Information on satellite tracks and statistical measures for comparing wind speed and significant wave height data

Track name	Track 1	Track 2	Track 3	Track 4
Storm	First	First	Second	Second
Satellite name	Sentinel 3A	Sentinel 3B	Sentinel 3A	Sentinel 3B
Passage time	Nov. 18, 2023, 19:01:51 UTC	Nov. 19, 2023, 08:41:18 UTC	Nov. 26, 2023, 18:54:21 UTC	Nov. 27, 2023, 08:33:50 UTC
Time relative to passage (s)	(+709) – (+783)	(-781) – (-696)	(+701) – (+781)	(−781) – (−703)
Statistical metrics for wind speed comparisons				
RMSE (m/s)	3.87	1.89	1.24	2.41
SI	0.27	0.09	0.06	0.16
Statistical metrics for significant wave height comparisons				
RMSE (m)	0.67	0.39	0.88	0.41
SI	0.31	0.04	0.10	0.09

as the land effects could introduce misleading results. To quantitatively compare the conformity between the data from the ERA5 dataset and the altimeters, widely-used statistical metrics root mean square error (*RMSE*) and scatter index (*SI*) are computed given by Eqs. 1 and 2:

$$RMSE = \sqrt{\frac{1}{N}\sum_{i=1}^{N}(O_i - P_i)^2} \quad (1)$$

$$SI = \sqrt{\frac{\sum_{i=1}^{N}((O_i - \overline{O}) - (P_i - \overline{P}))}{\sum_{i=1}^{N} O_i^2}} \quad (2)$$

In Eqs. 1 and 2, N is the number of data points, O is observations, $\overline{O}$ is mean of observations, P is predictions, and $\overline{P}$ is mean of predictions. In the present context, observations and predictions correspond to the altimeter measurements (i.e., Sentinel 3A and Sentinel 3B data) and reanalysis data (i.e., ECMWF-ERA5 dataset), respectively.

In Fig. 3, the interpolated ERA5 wind speed data is compared with the altimeter wind speed data, and *RMSE* and *SI* values are presented in Table 1. The results indicate that the ERA5 and Sentinel-3A and 3B altimeter data are mostly in reasonable agreement, also observed in the statistical metrics. However, the ERA5 dataset slightly underestimates the Sentinel-3A data during the first storm (Track 1 in Fig. 3a) and the Sentinel-3B data during the second storm (Track 4 in Fig. 3b). These slight discrepancies might be due to potential uncertainties introduced by the interpolation process, in addition to uncertainties inherent in altimeter measurements and modeling (ERA5 dataset). Acknowledging these slight discrepancies, the wind speed and direction data retrieved from the ERA5 reanalysis dataset are used in further discussions to illustrate the variations across the Black Sea.

In Fig. 4, the spatial distribution of wind speeds and directions based on the ERA5 reanalysis dataset are plotted at selected dates and times for the first storm (November 18–19, 2023), where the storm-affected regions are indicated with green and red shoreline segments corresponding to the first and second storms. It is observed that the first storm was largely effective in the Western Black Sea region for a duration of 21 h between November 18, 2023, 18:00 UTC and November 19, 2023, 15:00 UTC. The peak of the storm was reached around November 19, 2023, 03:00 UTC. The hourly wind speeds were more than 23 m/s in a region close to the Southern Black Sea coastline with a maximum of 23.9 m/s given at 42.0°N, 29.5°E. During the peak of the storm (Fig. 4d), the wind blew approximately from the northwest between longitudes 28.0E–30.5°E and latitudes 41.0°N–42.0°N, while it blew from the southwest between longitudes 31.5°E–34°E and latitudes 41°N–42.5°N. The storm center can be clearly seen in Fig. 4d in between the significant change of the wind directions. It is noted that hourly spatial distribution of wind speeds and directions are provided between November 18, 2023, 00:00 UTC and November 20, 2023, 00:00 UTC in the repository (see the Data Availability Statement).

Similarly, the spatial distribution of wind speeds and directions based on the ERA5 reanalysis dataset are presented at selected dates and times for the second storm (November 26–27, 2023) in Fig. 5, where the storm-affected regions are indicated with green and red shoreline segments corresponding to the first and second storms. It is observed that the second storm was mostly effective for a duration of 15 h between November 26, 2023, 09:00 UTC and November 27, 2023, 10:00 UTC in the whole Black Sea region. The highest wind speeds (more than 25 m/s at several locations) were observed on

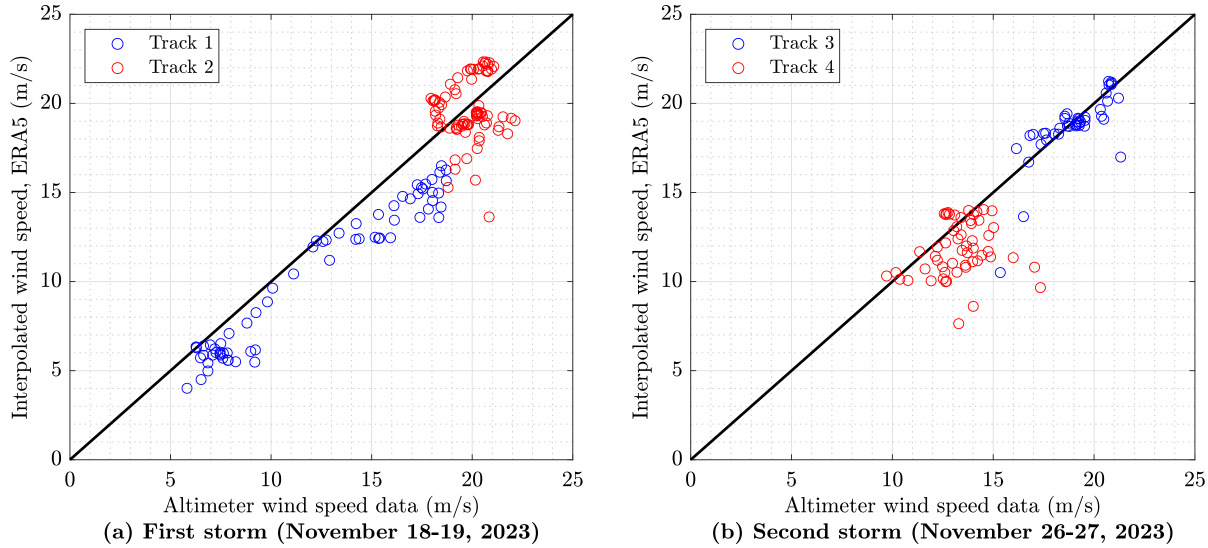

Figure 3
Comparison of the wind speed data retrieved from Sentinel 3A and 3B altimeters with the interpolated wind speed data from ECMWF-ERA5 dataset: **a** First storm (November 18–19, 2023), **b** second storm (November 26–27,2023). Details of the tracks are provided in Table 1.

November 26, 2023, 15:00 UTC in the Northwestern, Central and Southeastern Black Sea region (see Fig. 5c). The maximum wind speed was provided as 25.5 m/s on November 26, 2023, 15:00 UTC at 45.5°N, 31.0°E during the event. Relatively higher wind speeds were concentrated mainly at longitudes 31°E, 35°E and 37°E. In the Central Black Sea region, the wind direction was almost parallel to the coastline (i.e. blowing from west), whereas the wind blew from the northwest direction in the Eastern Black Sea region during the peak of the storm. It is noted that hourly spatial distribution of wind speeds and directions are provided between November 26, 2023, 00:00 UTC and November 28, 2023, 00:00 UTC in the repository (see the Data Availability Statement).

2.2. Wave Data

ECMWF's ERA5 reanalysis dataset provides significant height of combined wind waves and swell waves (SWH) and mean wave direction globally, having a spatial resolution of 0.5°. As there are no publicly available wave measurements during the event in the Black Sea region to the authors' knowledge, our investigation on the available wave data begins with a comparison of the ECMWF's ERA5 reanalysis dataset with altimeter observations. ERA5 reanalysis wave dataset is produced by wave modelling carried out using WAM model and assimilating data from altimeters namely ERS-1, ERS-2, ENVISAT, SARAL, JASON-1/2 and CRYOSAT-2 (ECMWF, 2016; Jiang, 2020). Alternatively, Sentinel 3A and 3B altimeters also provide significant wave height data, which is not included in the data assimilation procedure of ECMWF's ERA5 reanalysis dataset. It is again noted that the altimeter tracks during the storms and detailed information on those tracks are presented in Fig. 1a and Table 1, respectively. The comparisons were carried out based on the same methodology described in Section 2.1 for wind data. In Fig. 6, the interpolated ERA5 SWH data is compared with the altimeter significant wave height data for both storms. Additionally, the *RMSE* and *SI* values for each altimeter track are provided in Table 1. The results indicate that the ERA5 and Sentinel 3A and 3B altimeter data are in reasonably good agreement for both storms, despite potential uncertainties introduced by the interpolation process. Therefore, the SWH data retrieved from ERA5 reanalysis dataset is used in the further discussions.

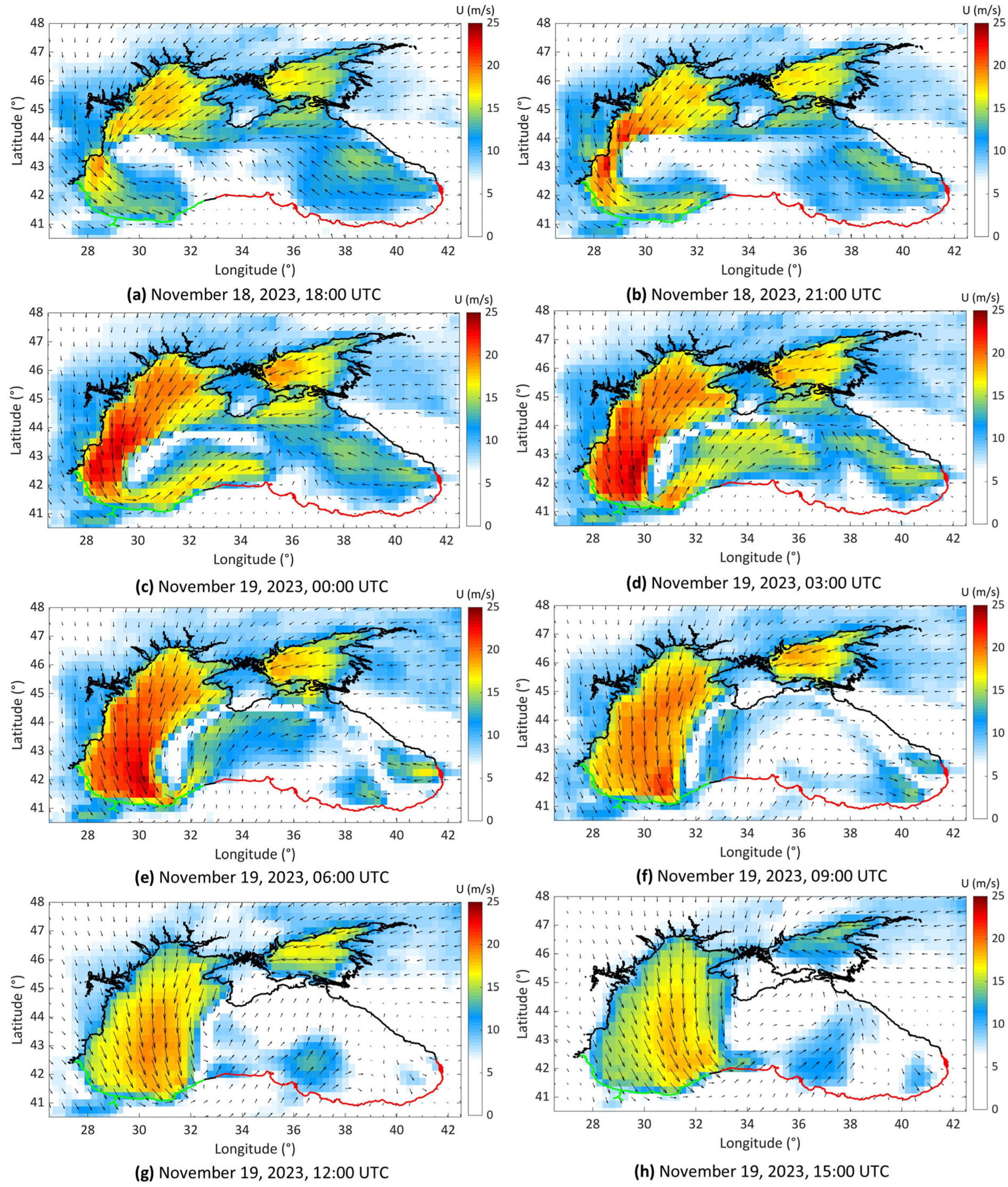

Figure 4
Distribution of wind speed magnitudes (U at 10 m above still water level) and directions for the first storm (November 18–19, 2023) based on the ECMWF-ERA5 reanalysis dataset over the Black Sea at the selected hours. (Green and red shoreline segments indicate the regions affected by the first (November 18–19, 2023) and second storms (November 26–27, 2023), respectively)

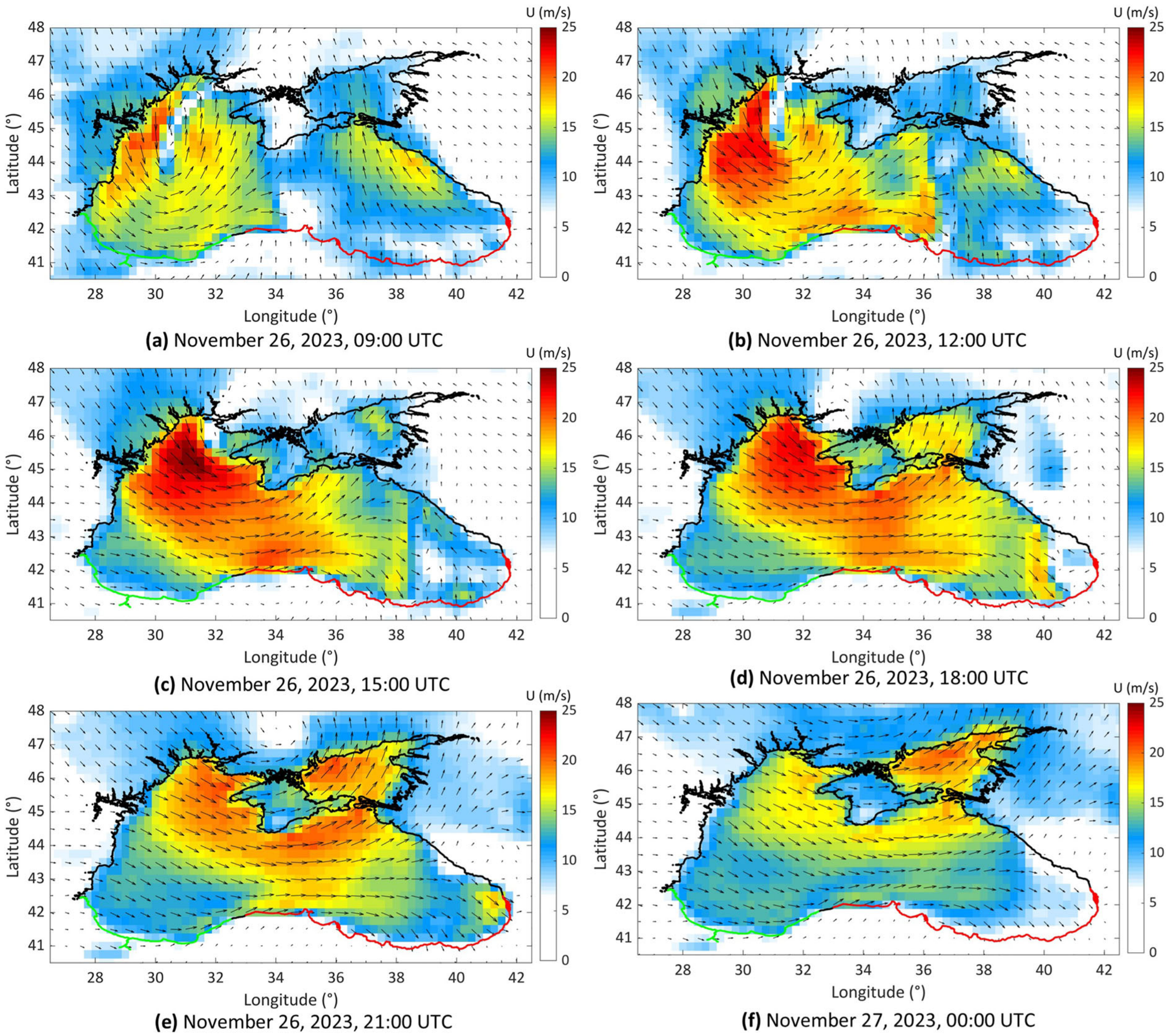

Figure 5

Distribution of wind speed magnitudes and directions for the second storm (November 26–27, 2023) based on the ECMWF-ERA5 reanalysis dataset over the Black Sea at the selected hours. (Green and red shoreline segments indicate the regions affected by the first (November 18–19, 2023) and second storms (November 26–27, 2023), respectively.)

In Fig. 7, the spatial distribution of ERA5 SWH data is provided at selected dates and times for the first storm (November 18–19, 2023), where the storm-affected regions are indicated with green and red shoreline segments corresponding to the first and second storms. The quiver plot shows the wave approach directions. It is observed that the SWH data higher than 4 m was estimated in the Western Black Sea region between November 18, 2023, 21:00 UTC (Fig. 7b) and November 19, 2023, 15:00 UTC (Fig. 7h). The SWH reached to its peak at November 19, 2023, 06:00 UTC, consistent with the timing of peak wind speed data (see Fig. 4), where SWH higher than 8 m was observed between longitudes 29°E–31°E and latitudes 41.5°N–43°N. It is noted that significant wave heights reaching up to 8 m were also recorded by Sentinel 3B altimeter Track 2 (see Fig. 7a). The maximum ERA5 SWH data predicted during the peak of the storm was 8.6 m at 42.0°N, 29.5°E, which is approximately 90 km away from the

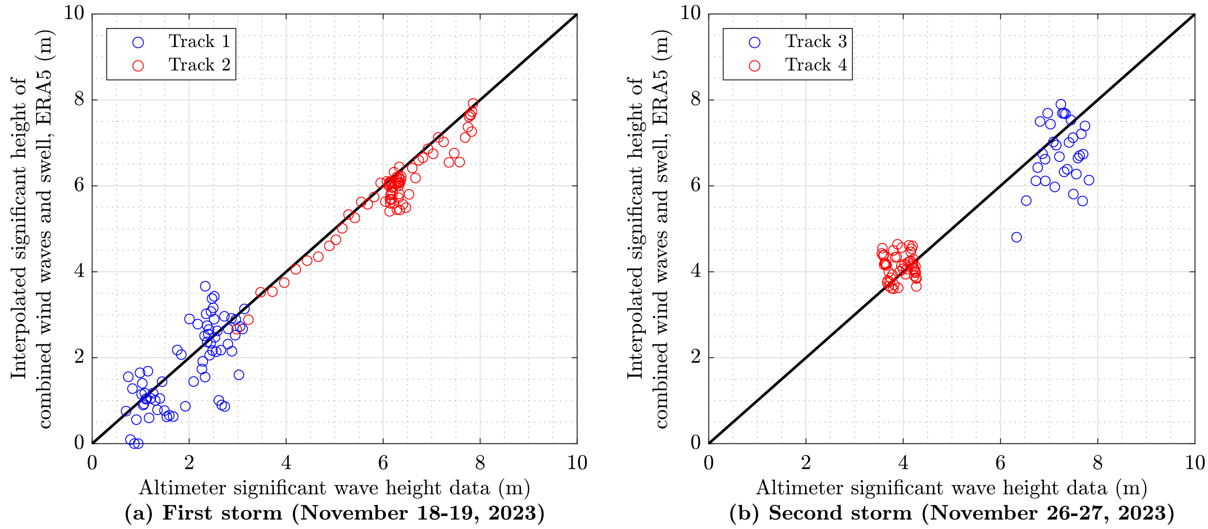

Figure 6
Comparison of the significant wave height data retrieved from Sentinel 3A and 3B altimeters with the interpolated significant height of combined wind waves and swell waves (SWH) data from ECMWF-ERA5 dataset: **a** First storm (November 18–19, 2023), **b** second storm (November 26–27,2023). Details of the tracks are provided in Table 1

shoreline. The waves approaching to the shoreline from the north and north-northwest directions during the peak of the storm in the Western Black Sea Region. The hourly spatial distribution of ERA5 SWH data is provided between November 18, 2023, 00:00 UTC and November 20, 2023, 00:00 UTC in the repository (see the Data Availability Statement).

On the other hand, the spatial distribution of ERA5 SWH data together with mean wave directions is provided at selected dates and times for the second storm (November 26–27, 2023) in Fig. 8, where the storm-affected regions are indicated with green and red shoreline segments corresponding to the first and second storms. In the Northwestern Black Sea region the SWH data was above 5 m at most of the data points between November 26, 2023, 12:00 UTC (Fig. 8b) and November 27, 2023, 00:00 UTC (Fig. 8f). On November 26, 2023, 18:00 UTC, the SWH data reached values more than 7.5 m, with a maximum of 7.9 m at 44.5°N, 32.0°E. Also, the Sentinel 3A altimeter measured significant wave heights up to 8 m along Track 3 (see Fig. 7b). The dominant mean wave direction was from west during the peak of the storm in the Central Black Sea region.

Although the storm had a severe impact on the Eastern Black Sea region (see the forthcoming Section 3), higher SWH values were predominantly observed in the Northwestern Black Sea, while only moderate SWH values (2–4 m) were recorded in the Eastern Black Sea region. This discrepancy suggests either that the ERA5 dataset failed to capture the storm event (might be due to underestimation of wind speeds) accurately in the Eastern Black Sea, or that a different meteorological phenomenon occurred in that area during the event. Unfortunately, no satellite altimeter tracks were available over the Eastern Black Sea during the event (see Fig. 1a). It is also noteworthy that video footage recorded during the storm shows relatively regular wave patterns along the shoreline, suggesting the presence of swell waves, as further discussed in Section 3.2.5. This observation highlights the need for more detailed numerical modeling of the storm, which is beyond the scope of the current field survey article. Therefore, no analysis based on ERA5 SWH data is provided for the Eastern Black Sea region. However, the hourly spatial distribution of ERA5 SWH data between November 26, 2023, 00:00 UTC and November 28, 2023, 00:00 UTC is included in the repository for the sake of completeness (see the Data Availability Statement).

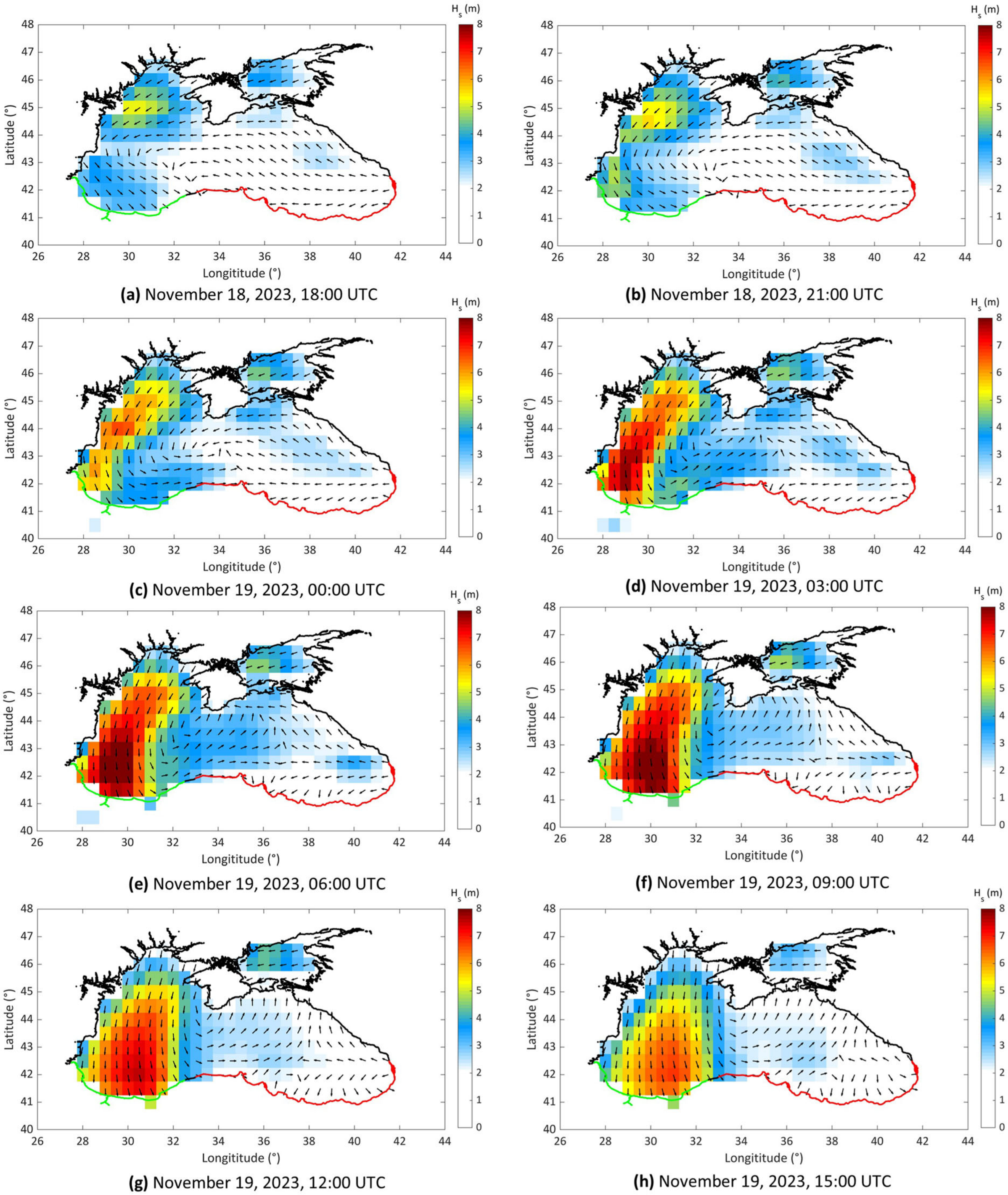

Figure 7

Distribution of significant height of combined wind waves and swell (SWH) for the first storm (November 18–19, 2023) based on ECMWF ERA5 reanalysis dataset over the Black Sea at the selected hours. (Green and red shoreline segments indicate the regions affected by the first (November 18–19, 2023) and second storms (November 26–27, 2023), respectively.)

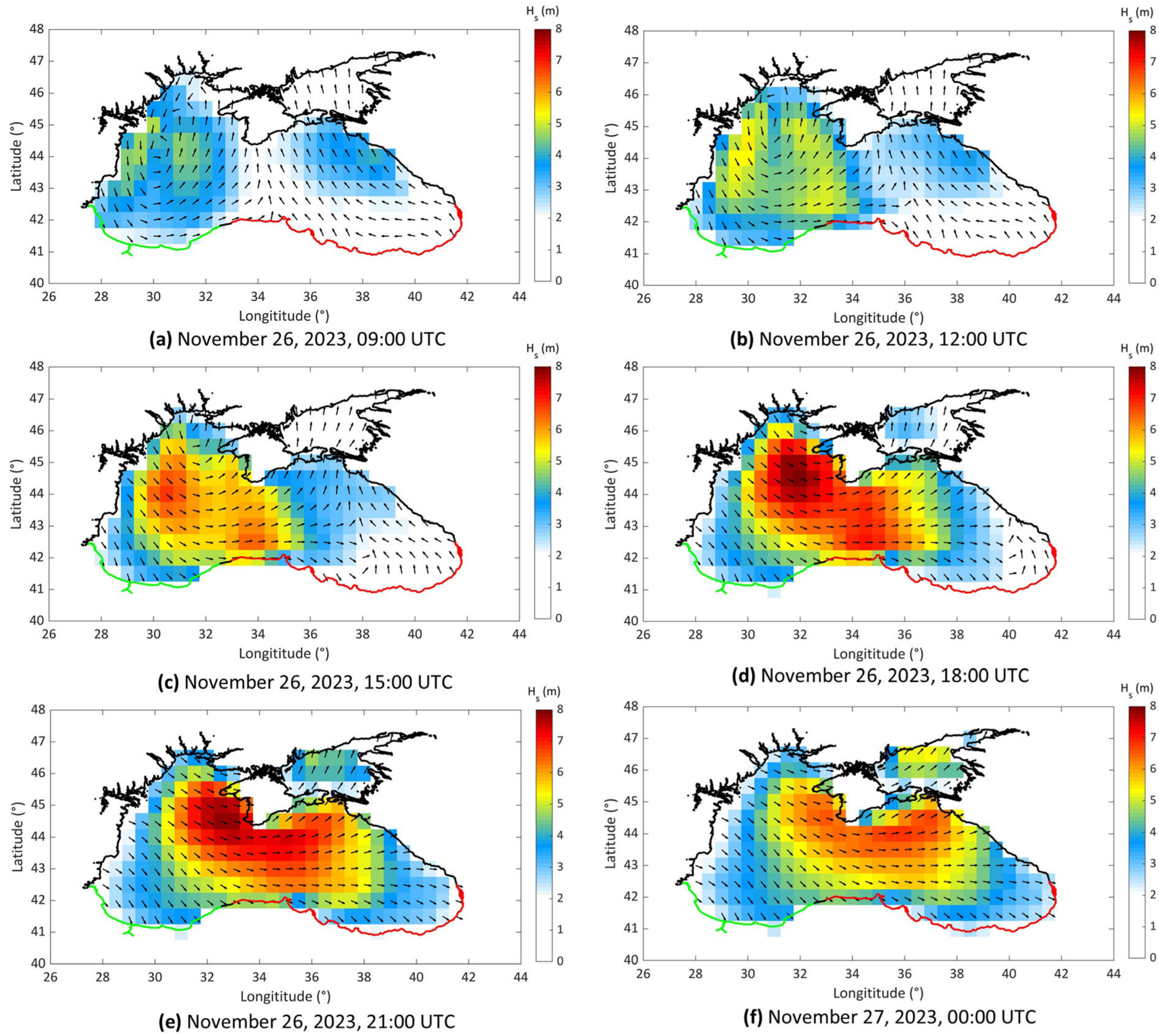

Figure 8
Distribution of significant height of combined wind waves and swell (SWH) for the second storm (November 26-27, 2023) based on ECMWF ERA5 reanalysis dataset over the Black Sea at the selected hours. (Green and red shoreline segments indicate the regions affected by the first (November 18-19, 2023) and second storms (November 26-27, 2023), respectively.)

2.3. Tide Gauge Records

Tide gauge records from five stations along the Southern Black Sea coast, from west to east: Igneada (TG1), Sile (TG2), Amasra (TG3), Sinop (TG4), and Trabzon (TG5), are analyzed using data obtained from the UNESCO-IOC Sea Level Monitoring Facility (http://www.ioc-sealevelmonitoring.org) (Fig. 1a and Table 2). The sea level measurements were recorded at 30-second intervals over a one-

Table 2

Coordinates of tide gauge stations

#	Station Name	Coordinate
TG1	Igneada	41.8889°N, 28.0235°E
TG2	Sile	41.1764°N, 29.6054°E
TG3	Amasra	41.7440°N, 32.3903°E
TG4	Sinop	42.0231°N, 35.1495°E
TG5	Trabzon	41.0020°N, 39.7446°E

month period, from November 5 to December 5, 2023. To process the raw data for analysis, first, a simple linear fit was applied to remove trends from the raw sea level series. Then, tidal signals were predicted using the TIDALFIT toolbox by Grinsted (2025), and subsequently removed to obtain detided records (Fig. 9a-e).

The resulting residual sea level time series, along with their long-period components ($T > 2$ hours, T being period), are shown in Fig. 10a-e. The long-period components in Fig. 10a-e reveal the occurrence of significant storm surges, with two prominent peaks observed across all stations. The first and more pronounced peak appeared on November 19, 2023, in Igneada and Sile; November 21 in Amasra (TG3) and Sinop (TG4); and November 23 in Trabzon (TG5), indicating a west-to-east propagation of the storm system. During the first event, the highest recorded sea level reached approximately 0.8 m in Sile (TG2), followed by approximately 0.4 m in Igneada (TG1) and $\sim$0.3 m at Amasra (TG3), Sinop (TG4), and Trabzon (TG5). These results highlight the greater storm surge intensity along the western Black Sea coast of Turkiye. The second peak was weaker, with non-tidal residual heights not exceeding $\sim$0.2 m at most stations, except for Trabzon (TG5), which experienced a maximum of $\sim$0.1 m.

In addition to the storm surges, high-frequency sea level oscillations (HFOs) intensified concurrently during both storm events, particularly at Sile (TG2),

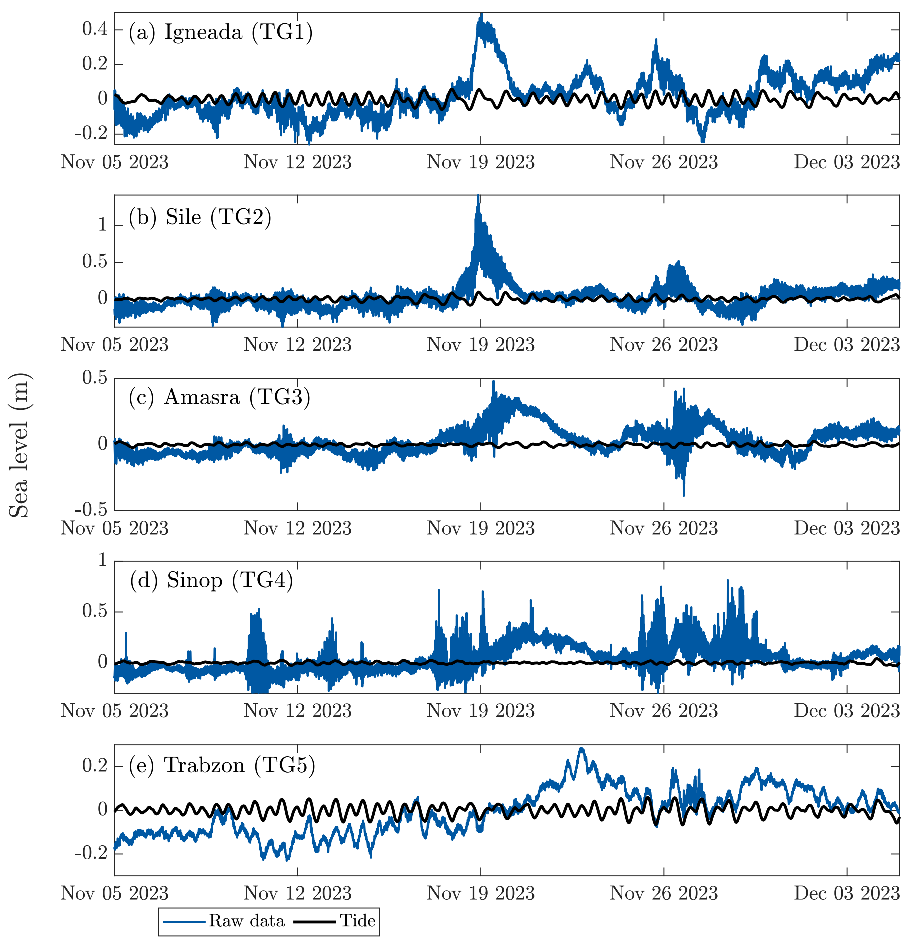

Figure 9
Analysis of tide gauge records for five tide gauge stations showing the recorded sea level and predicted tide. (a) Igneada (TG1), (b) Sile (TG2), (c) Amasra (TG3), (d) Sinop (TG4), (e) & (j) Trabzon (TG5)

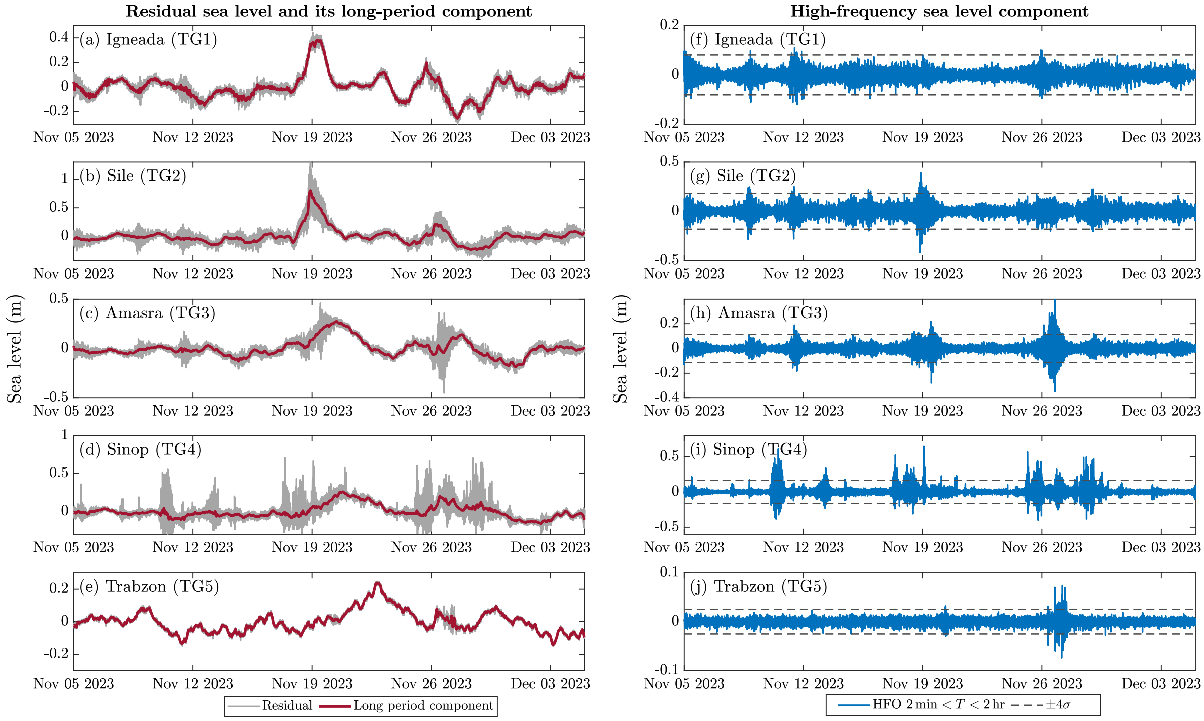

Figure 10
Analysis of tide gauge records for five tide gauge stations. The left-panel shows the residual sea level and its long-period components, and the right panel shows the isolated high-frequency sea level oscillations with periods between 2 min and 2 h, with four standard deviations (4σ) threshold used for meteotsunami identification (Monserrat et al., 2006). **a** & **f** Igneada (TG1), **b** & **g** Sile (TG2), **c** & **h** Amasra (TG3), **d** & **i** Sinop (TG4), **e** & **j** Trabzon (TG5)

and the central stations Amasra (TG3) and Sinop (TG4). As shown in the right panel of Fig. 10, these oscillations, corresponding to periods between 2 min and 2 h, locally reached amplitudes of up to approximately 0.4 m at Sile and Amasra and 0.7 m at Sinop, exceeding the four standard devitaion ($\pm 4\sigma$) threshold derived from the filtered records. This amplitude threshold is commonly used for identification of meteotsunamis, defined as meteorologically driven waves within the tsunami frequency band (Monserrat et al., 2006; Vilibić et al., 2025). These intensifications might suggest a meteotsunami; however, a definitive classification requires further investigation of the external forcing and the associated resonance mechanisms responsible for the local intensification at these stations. Nevertheless, the residual sea level increases substantially when such intense HFOs are accompanied by significant storm surges, and water levels within harbors may reach hazardous levels.

Overall, these analyses suggest that the extreme sea levels observed during the successive events in November 2023 were primarily driven by the superposition of storm surges and intensified HFOs, while tidal signals remain minimal in this microtidal region.

3. Field Observations

The field survey, conducted in four separate phases, covered most of the regions affected by both storms along the Southern Black Sea coastline, as illustrated in Fig. 1b-c. A summary of the field survey results is provided in Table 3, which includes the survey locations, dates, representative coordinates, measured inundation distances, and relevant notes. In this study, the inundation distance is defined as the horizontal distance from the coastline to the furthest point inland reached by the waves or surge.

Table 3

Summary of field survey results. Locations S1-S3 were affected from the first storm, whereas Locations S4-S22 were affected from the second storm

#	Survey location	Survey date	Coordinates	Inundation distance (m)	Notes
S1	Rumeli Fishery Harbor	Nov. 23, 2023	41.232326°N, 29.113631°E	–	see Sec. 3.1.1
S2	Sile Fishery Harbor	Jan. 21, 2024	41.180925°N, 29.607830°E	16	see Sec. 3.1.2
S3	Sile Fishery Harbor		41.179815°N, 29.611045°E	24	
S4	Inebolu Port	Jan. 7, 2024	41.980253°N, 33.764599°E	–	see Sec. 3.2.1
S5	Inebolu Teachers' Guesthouse		41.979454°N, 33.762044°E	59.7	
S6	Inebolu Office of Directorate Highways		41.977436°N, 33.736763°E	48.7	
S7	Inebolu Heyamola Restaurant		41.977329°N, 33.746414°E	25	
S8	Evrenye Fishery Harbor	Jan. 7, 2024	41.974312°N, 33.888477°E	–	Minor damage at the rear side of the main breakwater
S9	Ilisi Fishery Harbor	Jan. 7, 2024	41.980068°N, 33.968395°E	20	see Sec. 3.2.2
S10	Abana Fishery Harbor	Jan. 7, 2024	41.982303°N, 34.021627°E	–	see Sec. 3.2.3
S11	Tirebolu	Dec. 17, 2023	41.003292°N, 38.809109°E	270	see Sec. 3.2.4
S12	Tirebolu		41.007212°N, 38.812784°E	49	
S13	Tirebolu		41.005865°N, 38.809207°E	42	
S14	Yenicam Harbor	Dec. 17, 2023	40.922644°N, 40.187944°E	–	Minor damage at the rear side of the main breakwater
S15	Rize City Hospital	Dec. 16, 2023	41.050522°N, 40.602985°E	125	see Sec. 3.2.5
S16	Rize Gündoğdu/ Bozukkale Boat Yard	Dec. 16, 2023	41.059797°N, 40.624296°E	–	see Sec. 3.2.6
S17	Rize Tashane Fishery Harbor	Dec. 16, 2023	41.108054°N, 40.741742°E	-	Minor damage at the head section of the main breakwater
S18	Rize Ardesen Fishery Harbor	Dec. 16, 2023	41.195058°N, 40.985914°E	–	see Sec. 3.2.7
S19	Findikli	Dec. 16, 2023	41.271877°N, 41.139607°E	50	see Sec. 3.2.8
S20	Findikli		41.273544°N, 41.141811°E	15	
S21	Hopa	Dec. 16, 2023	41.401447°N, 41.425592°E	27	see Sec. 3.2.9
S22	Hopa Esenkıyı Fishery Harbor	Dec. 16, 2023	41.441378°N, 41.456037°E	–	No damage in this harbor

As a key component of this work, a digital repository was also developed to archive the material collected during the field surveys. This repository includes photographs and videos taken either by the survey team or by eyewitnesses to the events (see Data Availability Statement). The materials are organized by location, following the entries in Table 3, and each folder includes a "Read Me" file briefly describing the contents and acknowledging the data source. Throughout the manuscript, we refer to this repository for additional context on storm impacts, as it would be impractical to present the full extent of visual documentation within the main body of the paper.

The remainder of this section presents site-specific observations and analyses of the storm impacts at the most significantly affected locations. It is again noted that the two successive storms considered in the present study affected distinct regions along the Southern Black Sea coastline, as confirmed by the field surveys. In other words, the regions impacted by the second storm (see Fig. 1c) did not experience any effects from the first storm.

3.1. *Observations Regarding the First Storm on November 18-19, 2023*

3.1.1 *Rumeli Fishery Harbor*

Rumeli Fishery Harbor is located on the European side of the northern entrance to the Istanbul Bosphorus Strait and is denoted as S1 in Fig. 1b and in Table 3. According to the available wind and wave data evaluated in Section 2, wind speeds were over 23 m/s from the northwest whereas the significant wave height of combined wind waves and swell (SWH) was in the order of 8 m offshore the fishery harbor during the peak of the first storm.

Rumeli Fishery Harbor is protected by two mound breakwaters. The northern part of the main breakwater was constructed using cube units whereas the eastern side of the main breakwater was constructed using Antifer units. A closer view of the harbor in Google Earth is presented in Fig. 11a, where the approximately 130 m long red line indicates the region that was severely damaged by storm waves. During the event, the crown wall of the main breakwater failed along this marked region, noting that there was no observed damage in the armor layer (i.e., Antifer units). The cross-section of the crown wall is given in Fig. 11b based on the field measurements. The vertical part of the crown wall was constructed in three segments connected with reinforcement bars. The top two segments were overturned towards the harbor side due to severe wave action along the red line indicated in Fig. 11a. The photos of the overturned crown-wall segments are shown in Fig. 11c-d. The reason of this damage is most probably related to weakly anchored crown-wall segments (Fig. 11e), which failed to support forces caused by extreme wave action. This extreme wave action also caused overturning of the navigation beacon located at the head of the main breakwater (Fig. 11f). Additionally, a fisherman was swept into the sea by overtopping waves but was fortunately rescued, and the restaurant located at the northeastern corner of the harbor, on the top of the main breakwater, suffered extreme damage.

In the repository, additional photos from the Rumeli Fishery Harbor field survey, video footage taken during the event, and links to the news, including descriptive photos of the damage, are presented.

3.1.2 *Sile Fishery Harbor*

Sile Fishery Harbor is located in eastern Istanbul and is denoted as S2–S3 in Fig. 1b. Similar wind and wave characteristics to the Rumeli Fishery Harbor were estimated by the reanalysis dataset. The harbor is protected by two rubble mound breakwaters. Significant damage was observed on the rear side of the main breakwater due to extreme wave action (Fig. 12a). Additionally, the storm caused minor damage to a small shop located on the main breakwater (Fig. 12b). Inside the harbor, a small fishing boat sank as a result of storm waves that penetrated into the harbor area, noting that the mouth of the port is open to northwest direction.

To the east of the harbor, there is a natural bay. A rubble mound slope followed by recurved seawalls (+4.0 m above still water level, SWL) were constructed along the shoreline of this bay to protect the coastal road, which also provides access to the port area. In this region, significant wave overtopping was observed, leading to coastal inundation. The inundation distance at locations S2 and S3 were measured as 16 m and 24 m, respectively, also provided in Table 3.

The repository includes photos from Sile Fishery Harbor field survey as well as a link to a news article featuring video footage that shows the wave overtopping during the event.

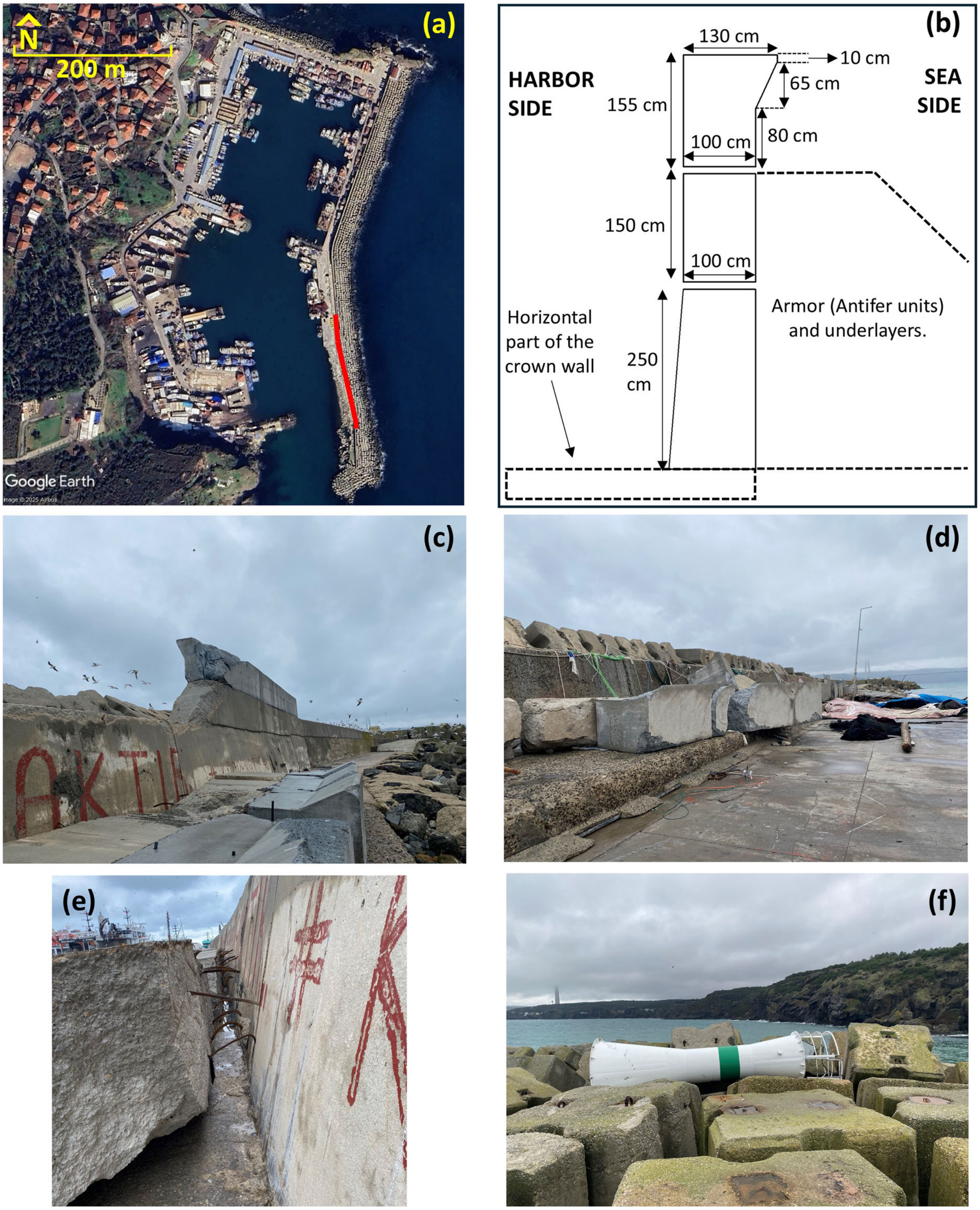
(a)
N
200 m
Google Earth
(b)
130 cm
10 cm
65 cm
HARBOR SIDE
SEA SIDE
155 cm
80 cm
100 cm
150 cm
100 cm
Horizontal part of the crown wall
250 cm
Armor (Antifer units) and underlayers.
(c)
(d)
(e)
(f)

◀Figure 11
Field survey at Rumeli Fishery Harbor: **a** Google Earth view of the harbor (Image taken on February 20, 2024), **b** cross-section of the crown-wall showing dimensions of its components (dimensions of the regions indicated by dashed lines are not known), **c** view of damaged crown-wall, **d** overturned crown-wall segments, **e** reinforcement bars vertically placed inside the crown-wall segments, **f** overturned navigation beacon

3.1.3 Eregli

Although the field survey team could not visit Eregli region, two important events occurred at Eregli Port (denoted as Eregli in Fig.1b), during the storm. Two vessels became unusable between 06:00 and 08:00 UTC on November 19, 2023. Based on the evaluated datasets presented in Section 2, the wind velocities were in the order of 17 m/s from southwest direction around the port area while the SWH offshore the port was approximately 5–6 m from northwest direction. Moreover, the storm center that could be observed in Fig. 4e was close to Eregli Port region.

During the event, the dry cargo ship Pallada, which was anchored at Eregli Port, failed to hold at anchor around 06:30 UTC as the storm intensified. The vessel subsequenltly dragged anchor and broke into two pieces. The two parts of the vessel were carried towards the shoreline, grounded, and fortunately the crew was successfully rescued (see NTV (2023) for the photos of the grounded vessel).

Meanwhile, another vessel Kafkametler was also dragged, and collided with the northern breakwater at Eregli Port. Unfortunately, the ship sank around 07:30 UTC, and all 12 crew members lost their lives. Additionally, the northern breakwater of the port suffered extensive damage (loss of armor layer units and overturning of crown walls towards sea side) due to both the storm conditions and the collision with the vessel (locally). In contrast, no significant damage was reported at the southern breakwater, which was constructed almost 50 years after the northern one.

3.2. Observations Regarding the Second Storm on November 26-27, 2023

3.2.1 Inebolu

Inebolu is a coastal town located in the Central Black Sea region and is denoted as S4–S7 in Fig. 1c. During the peak of the storm, wind speeds reached approximately 20–22 m/s from the west (almost parallel to the coastline). Offshore significant wave height (SWH) near Inebolu was around 6–7 m from west and west-northwest directions.

Inebolu Port was the first field survey location (denoted as S4 in Table 3) for the second storm. It is a historical port dating back to the 1880 s and was later extended for commercial purposes. The extension of the main breakwater was constructed using Antifer units. During the storm, a section approximately 80 m in length (in the extended part of the

Figure 12
Field survey at Sile Fishery Harbor: **a** Rear side damage of the main breakwater, **b** damaged small shop located at the crest of the breakwater

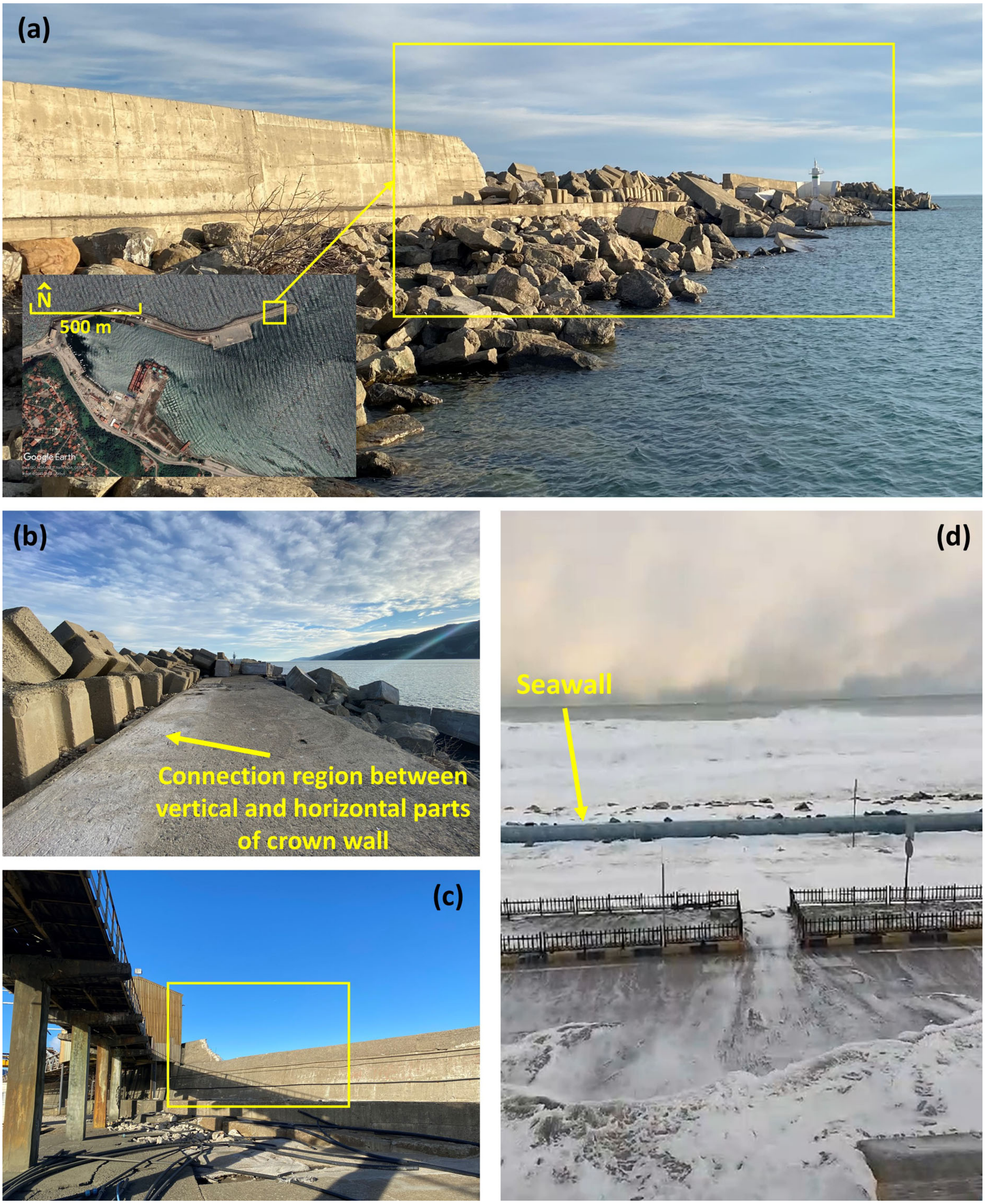

main breakwater) failed (Fig. 13a). The vertical part of the crown wall was washed away by wave action (Fig. 13b), and two Antifer units were dragged towards the harbor side. As shown in Fig. 13b, the connection (construction joint) between the vertical and horizontal parts of the crown wall appeared

◀Figure 13
Field survey at Inebolu: **a** Damage along the main breakwater of Inebolu Port. The failed section is indicated on the Google Earth view of the port (Image taken on July 2, 2021). **b** Close-up view of the failed section of the main breakwater (Inebolu Port), **c** view of damaged crown-wall (Inebolu Port), **d** snapshot showing inundation at Inebolu Teachers' Guesthouse (location S5), taken from video footage recorded by a witness (the video is included in the repository and named "S4-S7-video1")

almost flat, i.e., all the crown wall elements were swept away, suggesting a construction flaw in this area. The overtopped waves also caused damage to the rear side of the main breakwater, which was further exacerbated due to the failure of the vertical part of the crown wall. The security cameras in the main breakwater's berthing area, approximately at 22 m above still water level (SWL), failed during the event due to the splashing seawater, indicating huge wave overtopping rates. Additionally, the wall built atop the main breakwater's crown wall at a region near the shoreline to protect a conveyor belt in that area was broken by wave action, as shown in Fig. 13c.

The coastal road experienced widespread inundation during the storm. At the front of the Inebolu Teachers' Guesthouse (denoted as S5 in Table 3), waves overtopped a seawall with an elevation of 4.8 m above SWL (Fig.13d). This seawall is fronted by a rubble mound slope. The inundation distance measured at this location was 59.7 m. Similarly, at the Inebolu Office of the Directorate of Highways (denoted as S6 in Table 3), waves overtopped a seawall with an elevation of 5.1 m above SWL, damaging the fence atop the wall. The inundation distance here was measured as 48.7 m. Another surveyed area, location S7, experienced wave overtopping over a seawall with an elevation of 4.5 m, resulting in an inundation distance of 25 m. In this area, recreational coastal facilities, including restaurants and parks, suffered damage due to wave action.

The repository includes additional photos and video footages from Inebolu field survey. The videos include the full version of the snapshot presented in Fig. 13d.

3.2.2 *Ilisi Fishery Harbor*

Ilisi Fishery Harbor is a typical small harbor (Fig. 14a), located 15 km east of Inebolu Port. It is denoted as S9 in Fig. 1c and Table 3. During the event, wind and wave conditions offshore of this harbor were similar to those observed near Inebolu Port. Within the harbor area, there are several sheds along the southern berthing zone, a small sandy area on the eastern side, and a restaurant constructed atop the main breakwater at the northeastern corner of the port.

The restaurant, located 4.9 m above still water level (SWL), was severely damaged during the storm due to wave attack. The concrete slab in front of the restaurant was collapsed (Fig. 14b). The waves also displaced several rocks toward the harbor area, and the resulting debris accumulated in the sandy area inside the harbor (Fig.14c). During the event, waves penetrated inside the harbor overtopped the berthing places that are 0.75 m above SWL and inundated the sheds located in the southern part of the port. At the location indicated in Fig. 14a, the inundation distance was measured as 20 m.

On the other hand, moderate damage was observed along the main breakwater, which was constructed using cube blocks (Fig. 14d). Several cube units were displaced by waves, and the cube units that were placed adjacent to the crown wall were rotated as indicated in Fig. 14d using the yellow rectangle. This was most likely due to the displacement of supporting cube units on the seaward side of the rotated cube units.

The repository includes additional photos from the Ilisi Fishery Harbor field survey, showing the overall damage in further detail.

3.2.3 *Abana Fishery Harbor*

Abana is another coastal town located in the Central Black Sea region and is denoted as S10 in Fig. 1c and Table 3. The main breakwater of its fishery harbor experienced complete failure during the storm. Although inundation ranging from 80 to 100 meters was reported by local residents at locations other than the fishery port, this was not measured by the field survey team. The harbor was the main focus of the

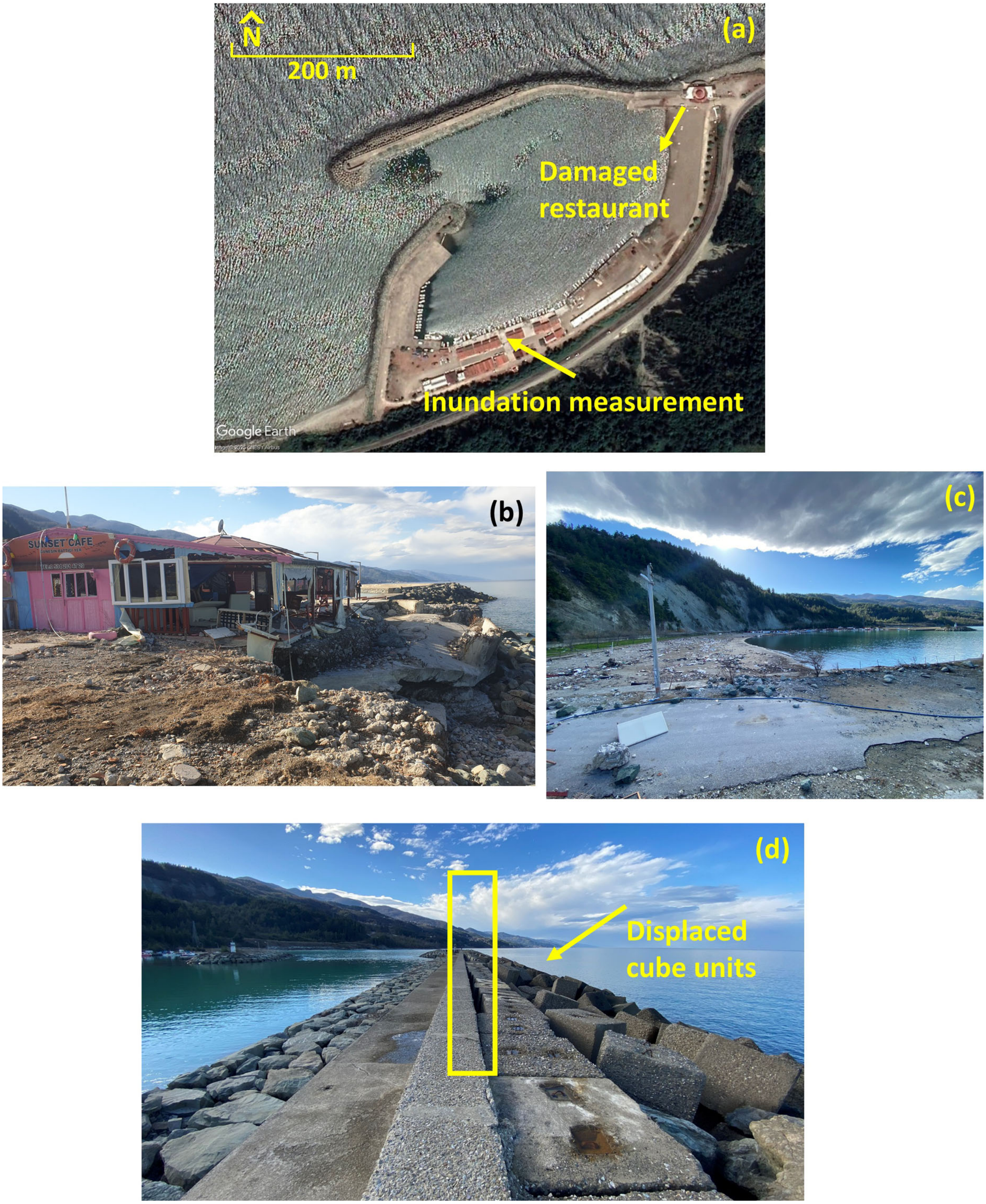

Figure 14
Field survey at Ilisi Fishery Harbor: **a** Google Earth view of the harbor (Image taken on July 2, 2021), **b** damaged restaurant, **c** view of the harbor area with debris accumulation along the beach, **d** minor damage at the main breakwater, where the yellow rectangle indicates the rotated cube units adjacent to the crown wall

field survey in Abana. Located approximately 5 km east of Ilisi Fishery Harbor, Abana experienced similar wind and wave conditions to those observed at Ilisi and Inebolu, as indicated by the data evaluated in Section 2.

The armor layer of the main breakwater at Abana Fishery Harbor was constructed using rock (along most of the trunk sections) and cube units (at the head section and the adjacent part of the trunk). The rock-armored trunk sections had already suffered extensive damage during previous storms, with much of the armor layer displaced. As a result, the crown walls in these sections were directly exposed to wave action. During the event, the vertical components of the crown walls in nearly all trunk sections were broken, overturned, and dragged into the harbor area (Fig. 15). In contrast, the sections armored with cube units experienced moderate damage, limited to the displacement of several units.

As shown in Fig.15a and b, Antifer units were present on top of the crown wall. At the time of the event, the main breakwater was being used as a storage area for these units, which were planned to be placed along the coastline of Abana and nearby towns for coastal protection against inundation. Most of the Antifer units remained stable under wave action, although two were displaced from the stockpile area. While the vertical components of the crown walls seaward of the Antifer units were not dragged into the harbor, most of them were still broken.

Additionally, sedimentation is a major ongoing problem for this harbor. In Fig. 15a and b, it can be seen that the gap between the main and secondary breakwaters is very narrow. Moreover, significant amount of sediment accumulated at the seaside of the main breakwater. These sedimentation issues are unrelated to the investigated storm event. Although the harbor entrance was well sheltered in this regard, the water level inside the harbor rose approximately 1 m during the event.

The repository includes additional photos and videos from field survey, including drone recordings before and just after the event.

3.2.4 Tirebolu

Tirebolu is a coastal city located in the eastern Black Sea region and is denoted as S11–S13 in Fig. 1c and Table 3. During the peak of the second storm in this area, the wind speeds reached up to 23 m/s from the northwest. It is noted again that SWH data has not been evaluated for the Eastern Black Sea region, starting with Tirebolu.

Significant inundation was observed at three locations in Tirebolu, as listed in Table 3. At Location S11, a small sandy beach with a mild slope was present, where the inundation distance reached approximately 270 meters. At Location S12, a seawall with an elevation of 2.5 meters above still water level (SWL) was constructed along the coastline. In this location, the inundation distance was measured as 49 meters. Facilities adjacent to the seawall, including a coffee shop and a market, were severely damaged during the event in this location. At the final surveyed site, Location S13, a seawall fronted by a rubble mound coastal protection structure having a crest elevation of approximately 5 meters above SWL was observed. Here, overtopping waves caused inundation extending 42 m.

The repository includes several photographs taken during the field survey, documenting the inundated areas, as well as video footage showing the extent of inundation.

3.2.5 Rize City Hospital Fill Area

Rize City Hospital is planned to be constructed on a fill area. The representative location is denoted as S15 in Fig. 1c and Table 3. During the storm event, the wind speeds in this region reached approximately 16–18 m/s from the northwest.

The fill area is protected by a sea dike composed of a mound slope armored with Antifer units and a crown wall. A cross-sectional sketch of the dike is presented in Fig. 16a, where two components of the crown wall are illustrated. Each crown wall strip had a length of 5.8 m (into the page). The crown wall components with a bullnose were not connected to the lower other components, i.e., the upper components remained stable due to their self-weight only (60.9 t assuming 2.4 t/m^3 of concrete density). Waves

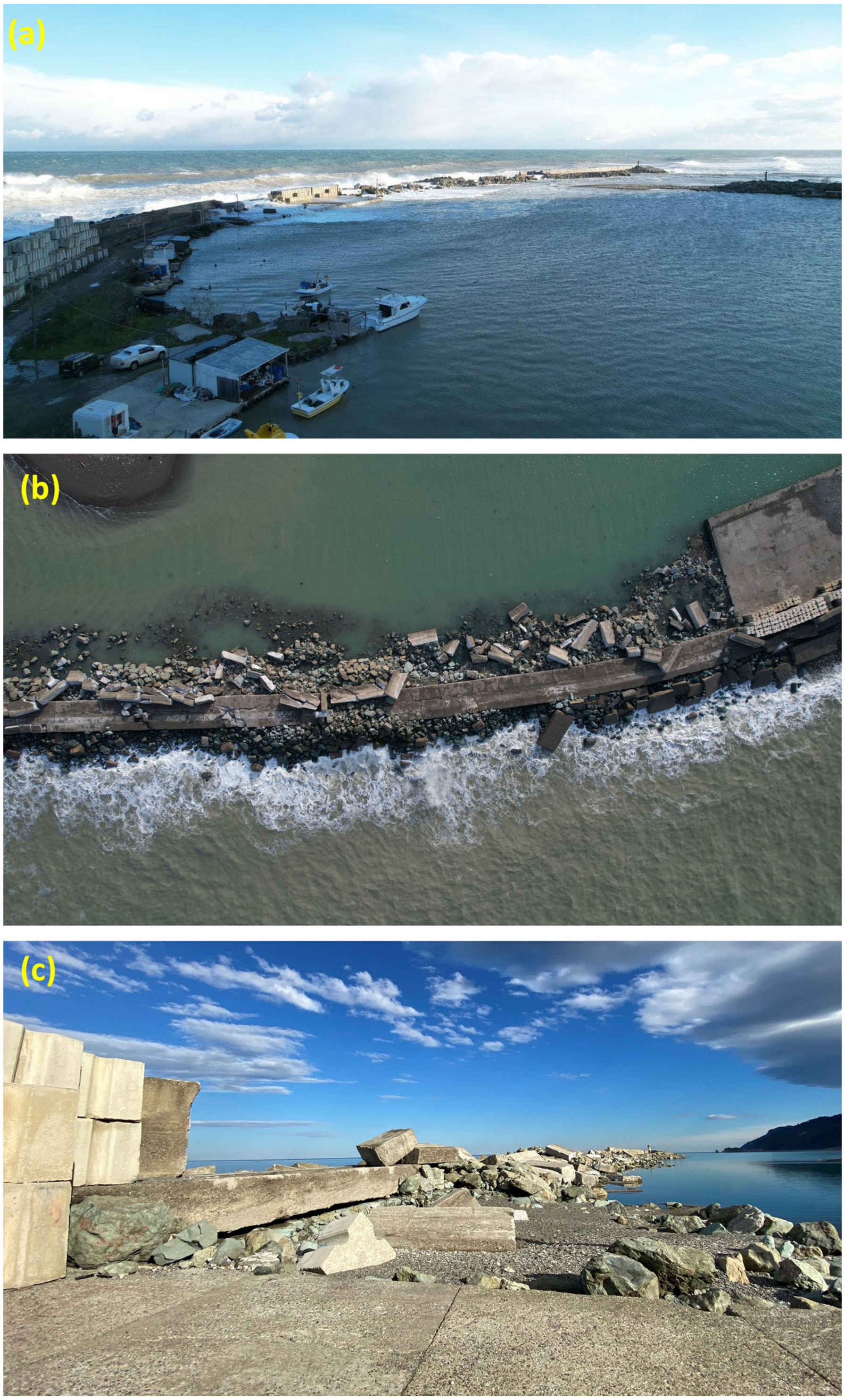

Figure 15
Field survey at Abana Fishery Harbor: **a** Damage along the main breakwater, **b** aerial view of failed trunk sections, **c** close-up view of the failed trunk sections. (Drone images were kindly provided by a local journalist called Semih Yuksel)

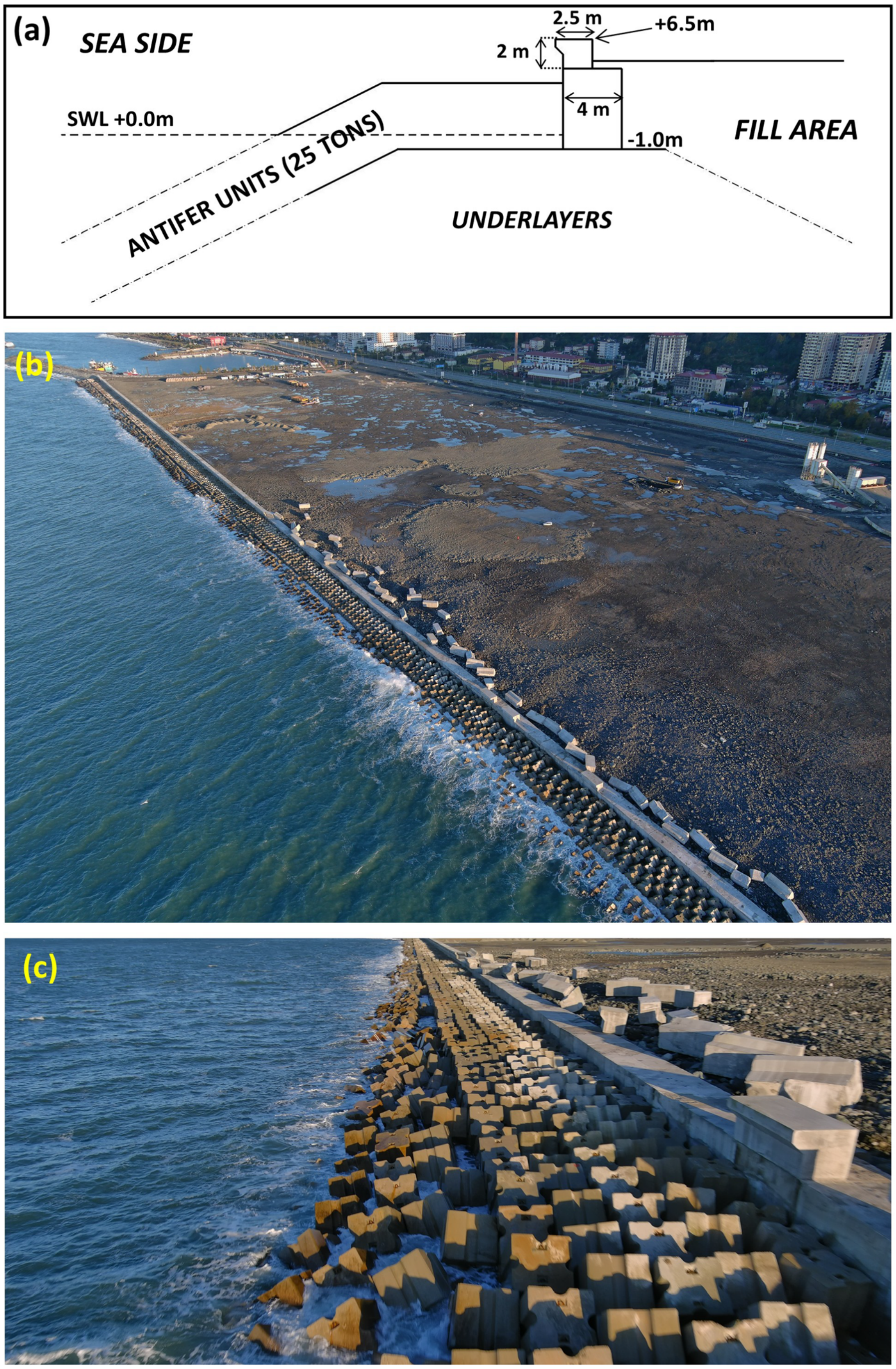

Figure 16
Field survey at Rize City Hospital Fill Area: **a** Sketch of the sea dike cross-section, **b** aerial view showing damage along the sea dike, **c** close-up view of the damaged section. (Drone images were kindly provided by Lead Engineer Akif Karanis from Ministry of Transport and Infrastructure, XI. Regional Directorate)

pushed these upper components towards the fill area (Fig. 16b and c). The sliding of the upper crown wall segments was observed along 400 m stretch of the sea dike. In the same region, some Antifer units were dislocated towards the seaward side, although those placed at the dike crest remained stable (Fig. 16c). It should be noted that there was no information whether the damage in the armor layer was related to this specific storm or not; however, it is most likely that the investigated storm caused the damage along the armor layer as this sea dike was newly constructed. Following the displacement of the upper crown wall segments, the fill area became more vulnerable to inundation, and the wave-induced inundation distance was measured as appromaximately 125 m.

The repository includes additional photos from the field survey. A video file (S15-video1) is also provided, capturing the wave action shortly after the upper crown wall units were dragged by wave action. As noted earlier in Section 2, the wave motion observed in this footage appears to be fairly regular, suggesting the presence of swell waves. However, this hypothesis requires further investigation through numerical modeling.

3.2.6 *Rize Gundogdu/Bozukkale Fishery Harbor*

Rize Gundogdu/Bozukkale Fishery Harbor is a typical small fishery harbor and is denoted as S16 in Fig. 1c and Table 3. As this harbor is located approximately 1 km east of the Rize City Hospital Fill Area, it was expected to experience similar wind and wave conditions during the event.

The main breakwater of this harbor was armored with rock units at the shallower trunk sections and with tetrapod units at the deeper sections (Fig.17a–b). During the storm, the crown wall of the main breakwater failed in multiple sections (Fig.17b–d). Several tetrapod units were displaced and thrown toward the harbor side, as marked with yellow in Fig.17b. Additionally, some rock armor units were thrown onto the crown wall (Fig.17b–d). The overtopping waves nearly destroyed the rear side of the breakwater.

Two distinct types of crown wall damage were observed at this location. In some sections, the vertical components of the crown walls were separated from the connection regions, overturned, and even pushed towards the harbor side (Fig.17c), similar to the damage observed at Rumeli Fishery Harbor (Section3.1.1), Inebolu Port (Section 3.2.1), Abana Fishery Harbor (Section 3.2.3), and the Rize City Hospital sea dike (Section 3.2.5). In contrast, other sections exhibited extensive breakage of the vertical crown wall elements (Fig. 17c, d, and f), which was not associated with the commonly weaker connection zones. This suggests a different failure mechanism, most likely linked to the impact of displaced tetrapod units. It is hypothesized that these tetrapods acted like hammers, striking and fracturing the crown wall units due to cyclic, wave-induced motion. A similar failure mechanism was previously documented during a severe storm in February 1960, which caused the breakage of tetrapod units at Crescent City Breakwater (Hudson, 1974).

It is noted that several additional photos from the field survey are provided in the repository.

3.2.7 *Ardesen Fishery Harbor*

Ardesen Fishery Harbor is located in the coastal city of Ardesen and is denoted as S18 in Fig.1c and Table 3. During the peak of the storm in this region, wind speeds were approximately 10–12 m/s from the northwest, relatively low compared to other surveyed locations. Nevertheless, extensive damage was observed at the harbor (Fig.18a–f), indicating that either the wind speeds eastward Ardesen were underestimated by ECMWF-ERA5 dataset or a different meteorological event occurred in the region that needs further investigation.

The main breakwater was constructed using Antifer units along the shallower trunk sections and rock armor at the deeper sections toward the head (Fig.18d), likely due to budget constraints. The vertical components of the crown wall were overturned at their connection points, particularly in the region where the armor layer consisted of rocks (Fig.18a, b, e, and f). The failure mechanism of crown wall is similar to what was observed at several previously investigated sites. The navigation beacon was also overturned during the event (Fig. 18c). The (weak) reinforcement bars connecting the horizontal

Figure 17
Field survey at Rize Gundogdu/Bozukkale Fishery Harbor: **a** Aerial view showing the damage at the main breakwater, **b** aerial view showing the damage at the main breakwater indicating the tetrapods thrown away to harbor side, **c** aerial view showing the overturned crown walls, **d** close-up view of the damage, **e** rocks thrown onto crown wall at shallower sections, **f** breakage of crown wall strips. (Drone images were kindly provided by Lead Engineer Akif Karanis from Ministry of Transport and Infrastructure, XI. Regional Directorate)

and vertical components are visible in Fig. 18f. The failure of the crown wall extended over a 111 m stretch along the main breakwater. In addition, the armor stones were thrown into the harbor, and the rear side of the breakwater was almost entirely destroyed.

◀Figure 18
Field survey at Ardesen Fishery Harbor: **a** and **b** Aerial view showing the damage at the main breakwater, **c** aerial view showing overturned navigation beacon, **d** aerial view showing the transition region from Antifer to rock armors, **e** close-up view of failed crown wall, **f** reinforcement bars along the overturned crown-wall segment. (Drone images were kindly provided by Lead Engineer Akif Karanis from Ministry of Transport and Infrastructure, XI. Regional Directorate)

Additional field survey photographs from Ardesen Fishery Harbor documenting the damage are provided in the repository.

3.2.8 Findikli

Findikli is a coastal town located in the eastern Black Sea region and is denoted as S19–20 in Fig. 1c and Table 3. During the peak of the second storm in this area, the wind speeds reached up to 13 m/s from the northwest, which might be underestimated by the investigated dataset.

Significant inundation was observed at two locations in Findikli (listed in Table 3), causing damage along the facilities near the coastal walking pathway. Additionally, the waves accumulated a significant amount of sediment at the estuary (41.268761°N - 41.137741°E), which was immediately removed by the municipality. At Location S19, a seawall with a crest elevation of 5.6 m above still water level (SWL) fronted by a rubble mound slope was overtopped by the waves. The inundation distance was measured as 50 m at this location. Moreover, a recreational facility at this location was significantly damaged by the waves. On the other hand, 15 m inundation distance was measured at Location S20, where a seawall having a crest elevation of 5.2 m above SWL was overtopped.

The repository includes several photographs taken during the field survey, documenting the damage and showing the locations where inundation distance measurements were carried out.

3.2.9 Hopa

Hopa is the easternmost location of the field survey and is denoted as S21 in Fig. 1c and Table 3. During the second storm, wind speeds reached up to 13–15 m/s from the northwest, according to the ECMWF-ERA5 dataset.

At that location, the waves were also effective and a vessel was grounded (Fig. 19). The seawall that can be seen in Fig. 19 has a crest elevation of 4.7 m above still water level (SWL). The waves overtopped the wall, and inundated the coastal road adjacent to the seawall. The total inundation distance was measured as 27 m.

4. Discussions and Conclusions

This study provides a detailed assessment of two successive severe storm events that impacted the southern Black Sea coast of Turkiye in November 2023. By combining analyses of available meteorological and oceanographic datasets with post-storm field surveys, the study documents the characteristics of these storms and their consequences on coastal structures and low-lying coastal areas. The first storm (18–19 November 2023) predominantly affected the western Black Sea region and lasted approximately 21 h, with peak wind speeds exceeding 23 m/s (northwesterly) and offshore significant wave heights (SWH) reaching 7–8 m. The second storm (26–27 November 2023) was slightly shorter in duration (15 h) but affected a wider stretch of the coastline, with wind speeds on the order of 20–22 m/s (westerly to northwesterly) and offshore wave heights around 6–7 m in the Central Black Sea basin. Both storms are clearly visible in tide gauge records spanning the entire southern coastline.

Although the study utilized well-established datasets, the analysis revealed some limitations in capturing the full impact of the events. For example, wave characteristics predicted by the ECMWF-ERA5 dataset for the eastern Black Sea exhibited inconsistencies with observed structural damage and coastal inundation. No dedicated hydrodynamic or wave model simulations were conducted as part of this work, as it was beyond the scope of the present study. However, the observed discrepancies in the evaluated datasets highlight the need for full numerical reproduction of such events, coupling atmospheric, wave, and surge models, to quantify coastal hydrodynamic

Figure 19
Grounded vessel in Hopa (Location S21)

processes. November 2023 storms led to significant coastal inundation and damage along the Southern Black Sea coastline, resulting in both human casualties and substantial economic losses. These events underscore the capacity of Black Sea storms to generate destructive waves and surge, confirming that even a semi-enclosed sea can experience extreme coastal hazards comparable to open-ocean coastlines.

Nearly all surveyed harbor sites experienced some form of damage in their coastal protection structures, especially the failure of crown walls. At multiple locations, crown walls on mound breakwaters were heavily damaged by the storm waves. In several cases, the vertical crown wall segments were overturned or sheared off at construction joints (interface between components of the crown-wall), apparently due to extreme wave pressures exceeding the structural capacity of their reinforcement. This mode of damage was observed (at Rumeli Fishery Harbor S1, Inebolu Port S4, Rize City Hospital S15, and Ardesen Fishery Harbor S18), highlighting a vulnerability in the design and/or construction of these coastal structures. In another instance (at Rize Gündoğdu Boat Yard S16), the impact from dislodged armor units played a crucial role in the damage, acting like a hammer. This second damage mechanism (mechanically induced breakage of the wall) was distinct from (yet co-occurred with) the overturning at weak joints. The consistency of these damage patterns across multiple sites suggests that crown walls are the most fragile component of many Black Sea breakwaters under extreme wave attack. This suggests the need to revisit the Turkish design and construction practices (and related manuals and guidelines), especially for crown walls.

The storms also caused severe wave overtopping and coastal inundation at numerous locations. Field measurements of inundation distances ranged from roughly 15–25 m in several towns (e.g., Sile S2–S3, Findikli S20) up to nearly 270 m inland at the worst-hit sites (Tirebolu S11). During the storms, even substantial seawalls (crest elevations on the order of 4.5–5.6 m above mean sea level) were overtopped by the storm surge and wave run-up. The extensive flooding of coastal roads, parks, and recreational structures is evidence of exceptionally high run-up elevations. The impact on coastal infrastructure was significant: several waterfront buildings (restaurants, harbor facilities, etc.) were destroyed or heavily damaged by wave action, and significant amounts of sediment and debris were deposited inland. The inundation measurements and damage evidence collected in this study provide valuable empirical data on the response of different coastal configurations to extreme overtopping, which can inform both hazard modeling and the design of future defenses. At present, design standards in Turkiye consider static design water levels. It could be argued that dynamic and/or scenario-based modeling, incorporating wave transformation analysis, is needed to enhance the resilience of coastal infrastructure in Turkiye.

In addition to structural damage on land, the storms posed important risks to vessels and maritime operations. The first storm's peak on November 19 coincided with a major accident at Eregli Port, where two ships were lost. These incidents emphasize that Black Sea storms can create perilous conditions not only for coastal infrastructure but also for ships at sea or at port, due to a combination of violent winds, high waves, and strong currents.

Overall, the extent and severity of damage observed in the November 2023 storms affirm that the Turkish Black Sea coast is highly vulnerable to extreme storm events. Ports and coastal communities along this shoreline have historically been among the most exposed to Black Sea storms (Amarouche et al., 2024), and the present field survey confirms that even relatively short-duration storms can inflict widespread destruction. A distinctive aspect of the November 2023 case is that two significant storms struck just one week apart. While these storms were separated by a brief calm period (and thus can be treated as distinct events), their back-to-back occurrence strained regional emergency response and drew attention to the possibility of sequential extremes. This indicates that the design standards and preparedness plans for the Black Sea coast must account for events of this magnitude.

Acknowledgements

The authors sincerely thank and gratefully acknowledge the contributions of Dr. Yalçın Eyigün (General Director) and Dr. Çaglar Tabak (Division Director) from the Ministry of Transport and Infrastructure, General Directorate of Infrastructure Investments, for providing comments on an early version of the manuscript. The authors extend their gratitude to Dr. Cuneyt Baykal from METU for reviewing the manuscript and providing insightful feedback. The authors also thank Bilge Karakutuk for her assistance in evaluating the tide gauge measurements. The authors express their gratitude to Lead Engineer Akif Karanis from the Ministry of Transport and Infrastructure, XI. Regional Directorate, and Semih Yüksel (local journalist) for providing drone imagery used to describe field observations. Special thanks are extended to the staff of Rize Findikli Municipality, Serife Teke, Engin Salci, and Oguzhan Dikici for their collaboration and assistance during the field survey, as well as for providing photos of the events as eyewitnesses. The authors also extend their sincere appreciation to Dr. Ceyla Inmeler, who contributed to the field survey on January 7, 2024. Finally, the in-situ wind data from coastal meteorological stations, provided by the Turkish State Meteorological Service, is gratefully acknowledged.

Author Contributions All authors contributed to the conceptualization and design of the study. Data collection was performed by H.G.G., G.G.D., I.G., S.P, and A.C.Y. Data analysis was performed by H.G.G., G.G.D., and C.K. The first draft of the manuscript was written by H.G.G. and G.G.D., and all authors commented on the previous versions of the manuscript. All authors read and approved the final manuscript.

Funding

Open access funding provided by the Scientific and Technological Research Council of Türkiye (TÜBİTAK). The authors declare that no funds, grants, or other financial support were received specifically for the study presented in this manuscript.The second author (Gozde Guney Dogan) acknowledges financial support from the Scientific and Technical Research Council of Turkiye (TUBITAK) under the 2219 International Postdoctoral Research Fellowship Programme.

Data Availability

The field survey dataset used in the present paper can be downloaded from Zenodo open database using the following address: https://doi.org/10.5281/zenodo.18327182.

Declarations

Conflict of interest The authors declare no conflict of interest.

REFERENCES

Amarouche, K., Akpınar, A., & Acar, E. (2024). Characterisation of wave storms events and their long-term variability off the key ports and shipping routes in the Black Sea. *Ocean Engineering, 297*, Article 116893. https://doi.org/10.1016/j.oceaneng.2024.116893

Aydin, D. C. (2016). Surge and coastal inundation study of September 2014 storm in Giresun, Black Sea. Msc thesis, Middle East Technical University, Ankara, Turkey.

Bernardino, M., Rusu, L., & Soares, C. G. (2021). Evaluation of extreme storm waves in the Black Sea. *Journal of Operational Oceanography, 14*(2), 114–128. https://doi.org/10.1080/1755876X.2020.1736748

ECMWF. (2016). IFS Documentation - Cy41r2. Part VII: ECMWF wave model. Reading, England: ECMWF.

Fashchuk, D. Y. (2011). *Wreck of the Tanker Volgoneft-139 in the Kerch Strait* (pp. 391–427). Springer.

Grinsted, A. (2025). Tidal fitting toolbox. MATLAB Central File Exchange.

Guler, H. G., Kirezci, C., Baykal, C., Ozyurt Tarakcioglu, G., Isik, E., Ergin, A., Yalciner, A. C., & Guler, I. (2024). Storm damage assessment of a port in the Southwestern Black Sea. *Coastal Eng, 192*, Article 104544. https://doi.org/10.1016/j.coastaleng.2024.104544

Hersbach, H., Bell, B., Berrisford, P., Hirahara, S., Horányi, A., Muñoz-Sabater, J., Nicolas, J., et al. (2020). The ERA5 global reanalysis. *Quarterly Journal of the Royal Meteorological Society, 146*(730), 1999–2049. https://doi.org/10.1002/qj.3803

Hudson, R. Y. (Ed.). (1974). *Conrete armor units for protection against wave attack: Report of ad hoc committee on artificial armor units for coastal structures*. US Army Corps.

Jiang, H. (2020). Evaluation of altimeter undersampling in estimating global wind and wave climate using virtual observation. *Remote Sensing of Environment, 245*, Article 111840. https://doi.org/10.1016/j.rse.2020.111840

Monserrat, S., Vilibic, I., & Rabinovich, A. (2006). Meteotsunamis: atmospherically induced destructive ocean waves in the tsunami frequency band. *Natural Hazards and Earth System Sciences, 6*(6), 1035–1051. https://doi.org/10.5194/nhess-6-1035-2006

NTV. (2023). News about the Pallada vessel incident appeared in national media NTV news. www.ntv.com.tr/galeri/turkiye/firtinada-ikiye-yarilan-gemi-havadan-goruntulendi,I5mUCpx78E-t7N5KHs5nlg/hDuMrVeyJkKjM5JEBPdiag (Last access: April 2, 2025).

Ranguelov, B., Tinti, S., Pagnoni, G., Tonini, R., Zaniboni, F., & Armigliato, A. (2008). The nonseismic tsunami observed in the bulgarian black sea on 7 May 2007: Was it due to a submarine landslide? *Geophysical Research Letters*. https://doi.org/10.1029/2008GL034905

Vilibić, I., Zemunik Selak, P., & Šepić, J. (2025). Meteorological tsunamis: From local hazard to global relevance. *Reviews of Geophysics, 63*(4), Article e2024RG000867. https://doi.org/10.1029/2024RG000867

Vilibić, I., Šepić, J., Ranguelov, B., Mahović, N. S., & Tinti, S. (2010). Possible atmospheric origin of the 7 May 2007 western Black Sea shelf tsunami event. *Journal of Geophy Research: Oceans, 115*, 07006. https://doi.org/10.1029/2009JC005904

(Received August 7, 2025, revised March 23, 2026, accepted May 9, 2026, Published online June 8, 2026)